An ancestral transmembrane transcription factor couples cell envelope regulation and the SOS response in *Caulobacter crescentus*

Kamilla Ankær Brejndal[1], Nikolaj Vestergaard Hansen[1], Koyel Ghosh[1], Sebastian Nielsen[1], Lykke Haastrup Hansen[1], Lene A. Jakobsen[1], Martin R. Larsen[1] and Clare L. Kirkpatrick[1]*

[1] Department of Biochemistry and Molecular Biology, University of Southern Denmark, Odense, Denmark.

* Corresponding author. Email clarek@bmb.sdu.dk ORCiD 0000-0001-8564-8559.

Short title: HigX regulates cell envelope genes

Keywords: antibiotic resistance, cell envelope, transmembrane transcription factor, toxin-antitoxin system, gene regulation, Caulobacter crescentus

Abstract

The DNA damage (SOS) response in bacteria involves derepression of a set of genes in order to activate mechanisms to tolerate stress, repair DNA and slow down cell division. While some of these genes are well characterized, many genes exist which are clearly induced by DNA damage but for which the function is unclear. In *Caulobacter crescentus*, the toxin-antitoxin (TA) system *higBA* and a closely associated downstream transcription factor (*higX*) are strongly induced as part of the SOS response, but the role of *higX* is unknown. We show that, unexpectedly, HigX functions independently of HigBA as a cell membrane-associated regulator and is toxic when overexpressed in filamentous cells. ChIP-Seq indicated that it binds to several promoters associated with cell envelope regulation. In cells with the SOS response constitutively activated, HigX was overproduced, but at the same time was unable to bind the majority of its target promoters. *higX* was highly conserved in genomic context among many alpha-proteobacteria, while *higBA* was only found upstream of it in a small number of *Caulobacter* genomes, including the universal laboratory strain *C. crescentus* NA1000. Compositional analysis suggested that *higBA* originated from a foreign source, while *higX* is likely ancestral to the alpha-proteobacteria. Our data support a model where dysregulation of HigX production and activity in filamentous Δ*lexA* cells contributes to cell envelope instability and antibiotic sensitivity. Thus, the protective effect of inhibiting cell division during the SOS response in order to repair the DNA, carries the hidden cost of interference with HigX-mediated cell envelope maintenance.

Author summary

The DNA damage (SOS) response in bacteria is key for their survival in harsh conditions, but the genes which are induced by this response and the molecular mechanisms involved are variable between different bacteria. We investigated the function of an uncharacterized SOS-induced gene in *Caulobacter crescentus* (*higX*) and found that it is a membrane-localized DNA binding protein, but that it did not help survival in DNA damage. Instead, it negatively affected cell viability when induced, unlike other SOS response genes. Genomic analysis showed that *higX* is highly

43 conserved among alphaproteobacteria, but it is only under SOS control in a small number of
44 genomes (including *Caulobacter crescentus*) where a toxin-antitoxin system and its SOS-
45 regulatory promoter have been inserted upstream. This work uncovers HigX as a novel factor in
46 cell envelope regulation, and shows that loss of cell shape regulation, eg. in filamentous Δ*lexA*
47 cells, can influence the ability of transmembrane transcription factors to bind to their target genes.

48

49 Introduction

50 Free-living bacteria require robust stress response systems in order to thrive in variable (and
51 sometimes stressful) natural environments. One of the most important is the SOS response
52 system, for response to and repair of DNA damage, especially double-strand breaks (1). When
53 DNA damage occurs, the SOS response allows cell division to be paused for the cell to carry out
54 DNA repair, in order to assure that intact chromosomes are passed on to the next generation.
55 LexA and RecA are the key regulators of the SOS response, and are widely conserved
56 among bacteria (2). In a noninduced state, LexA maintains its target genes under tight
57 repression by binding to specific recognition sites in their promoters. During DNA damage, RecA
58 recognizes single-stranded DNA and polymerises into a filament (3, 4). The polymer form of RecA
59 interacts with LexA causing it to cleave itself and leave the promoters, allowing transcription of the
60 target genes (5). While the consensus binding sequence for LexA varies between different
61 bacterial species, it is generally true that the closer a given LexA binding site matches the
62 consensus, the higher the affinity of LexA for the site and the tighter the repression of the
63 promoter(6). Hence, a high-affinity site can act as an on-off switch for its target genes, while a low-
64 affinity site would have a more subtle effect on transcription.

65 Toxin-antitoxin (TA) systems are widespread in bacterial genomes, with a tendency towards free-
66 living bacteria possessing multiple systems (frequently in multiple copies) and intracellular bacteria
67 having few or none (7). All systems consist of at least a toxin, which acts intracellularly to inhibit
68 central metabolism, and an antitoxin which inhibits toxin action (8-11). In some cases, described

69 further later, a third component is also present. The regulation of TA system activity is primarily
70 post-translational, because while the promoters of some TA systems are transcriptionally activated
71 by stress (12-15), transcriptional activation does not automatically result in a net increase of toxin
72 activity (16) and other systems are transcriptionally stress-insensitive (17, 18). In some bacteria,
73 TA system promoters are under the control of LexA (12-15). One example is the *higBA* system
74 of *Caulobacter crescentus*. This TA system comprises the DNA-binding protein antitoxin HigA and
75 the ribosome-dependent RNase toxin HigB and is negatively regulated by binding of HigA and
76 LexA upstream of the *higB* start codon. LexA binding to the *higBA* promoter provides sufficiently
77 strong repression that it is possible to delete the HigA antitoxin without major phenotypic
78 effects(15). Consistent with this, the LexA binding site in the *higBA* promoter is a perfect match
79 to the experimentally defined consensus sequence for *Caulobacter* LexA (19) (T/A)TGTTC
80 (N_6)TGTTC, and the HigA protein is almost undetectable in wild type (WT) *Caulobacter crescentus*
81 but strongly upregulated in the Δ*lexA* mutant (15). Due to this strict repression, HigB-dependent
82 phenotypes are most clearly observable in the Δ*lexA* mutant. In this strain, improvements in growth
83 rate and in ciprofloxacin resistance are seen when the *higB* toxin gene is deleted, suggesting that
84 the *higBA* TA system is a functional component of the *Caulobacter crescentus* DNA damage
85 response and that HigB's toxic activity contributes to poor growth rate and ciprofloxacin sensitivity
86 in Δ*lexA* cells. Hence, *Caulobacter crescentus higBA* is an example of a TA system in which
87 transcriptional derepression of its promoter (during DNA damage) does lead to toxin-dependent
88 phenotypes(15).

89 One toxin-dependent phenotype of the HigBA system was an unexpected protective effect against
90 cell envelope stress. This came to light through a forward genetic screen for rescue of nalidixic
91 acid sensitivity in the Δ*tipN* mutant, which identified *higA* as a loss of function suppressor
92 candidate, during a transposon insertion screen for nalidixic acid resistance (15). The mechanism
93 of this protective effect proved to be through HigB-mediated cleavage of the *acrB2* efflux pump
94 transcript mRNA, which was strongly transcriptionally induced by nalidixic acid. Mutants lacking

95 TipN had destabilized cell envelopes which were disproportionally sensitive to cell envelope stress
96 induced by overload of the envelope with AcrAB2 efflux pump proteins (20), unless these were
97 post-transcriptionally downregulated by HigB.

98 While our previous work focused on the role of HigB in the DNA damage and cell envelope stress
99 responses, it also came to our attention that other factors may be involved. In particular, we noted
100 different antibiotic resistance phenotypes for the Δ*lexA* Δ*higB* and the Δ*lexA* Δ*higBA* mutants, even
101 though both of these are lacking the toxin gene *higB*. The Δ*lexA* Δ*higBA* strain remained as
102 sensitive to DNA damaging antibiotics as the Δ*lexA* parent strain, and did not display the improved
103 resistance seen in the Δ*lexA* Δ*higB* mutant (15). To investigate sources of this HigB-independent
104 antibiotic sensitivity, we examined the genomic context of the *higBA* TA system and observed that
105 a third gene is encoded only 42 bp downstream of the *higA* antitoxin gene. The close proximity of
106 this gene (CCNA_03131) to *higBA* was suggestive of a function as a regulatory third component of
107 the TA system. However, it bore no similarity to the chaperone third components seen in other
108 *higBA* systems, in some cases designated *higC* (21, 22). Instead, it is annotated as a transcription
109 factor of the LytTR family. These factors are found in a wide variety of bacteria, including
110 pathogens, and regulate processes such as competence, extracellular toxin and bacteriocin
111 production, alginate production and quorum sensing (23). Here we show that this gene, for which
112 we propose the designation *higX*, (considering its close association with *higBA* but still enigmatic
113 function) is indeed a transcription factor and can regulate the TA system promoter, but its primary
114 function is independent from it. In evolutionary terms, *higBA* in *Caulobacter crescentus* is a recent
115 arrival upstream of *higX*. Insertion of *higBA* and its LexA-dependent promoter at this position is
116 unique to the *crescentus/vibrioides* lineage and is not conserved among other *Caulobacter* species
117 or other alpha-proteobacteria. Conversely, *higX* is widely conserved among the
118 alphaproteobacteria, generally found adjacent to a putative hydrolase gene and is not LexA-
119 dependent. Overproduction of *higX* upon LexA derepression in *Caulobacter crescentus* leads to
120 ciprofloxacin sensitivity, likely because the cell envelope is destabilized and the antibiotic has

121 easier access to its target inside the cell. However, we also observed that in the Δ*lexA* strain,
122 binding of HigX to its target promoters was globally decreased, suggesting a novel link between
123 cell filamentation and cell envelope gene regulation.

124 Results

125 Ciprofloxacin sensitivity of the ΔlexA ΔhigBA mutant is due to excessive production of a 126 transcription factor downstream of higBA

127 To investigate the source of the unexpected HigB-independent ciprofloxacin sensitivity in Δ*lexA*
128 Δ*higBA*, we focused on the CCNA_03131 (hereafter, *higX*) gene downstream of *higBA* (Fig. 1A).
129 We constructed in-frame deletions of *higX* in WT, Δ*lexA* or Δ*higBA* strains and investigated the
130 effect on ciprofloxacin sensitivity. Consistent with our previous observations (15), loss of *higA* in
131 the WT background sensitized cells to ciprofloxacin (through HigB activation), while deletion of
132 *higB* from the Δ*lexA* strain was protective against it. Deletion of *higX* in WT, with or without deletion
133 of *higBA*, had no effect. However, in the ciprofloxacin-sensitive Δ*lexA* Δ*higBA* background, deletion
134 of *higX* improved ciprofloxacin resistance to a similar level to the Δ*lexA* Δ*higB* strain, showing that
135 *higX* is indeed responsible for the ciprofloxacin sensitivity in the Δ*lexA* Δ*higBA* strain in the
136 absence of the HigB toxin (Fig. 1B).

137 The Δ*lexA* Δ*higBA* strain had been constructed by in frame deletion of *higBA* in the Δ*lexA* single
138 mutant background. However, we subsequently realized that this would exert polar regulatory
139 effects on *higX* expression, because (1) deletion of the *higBA* coding sequence brings *higX* directly
140 downstream of the strong promoter regulating *higBA*, and (2) both repressors of this promoter,
141 LexA and HigA, are absent. Indeed, we observed that *higX* was transcribed at very low levels in
142 WT, Δ*higA* and Δ*higBA* but much higher in Δ*lexA* Δ*higBA* (Fig. 1C). Therefore, the ciprofloxacin
143 sensitivity phenotype of Δ*lexA* Δ*higBA* is associated with elevated HigX RNA expression,
144 suggesting why *higX* deletion is protective.

145

146 ## HigX regulates the expression of higBA alongside LexA and HigA

147 In other three-component TA systems with a transcription factor as their third component, the
148 transcription factor regulates of the promoter upstream of the TA system (18, 24). To investigate
149 whether HigX also has this activity, we examined activity of a transcriptional P_{higBA}-*lacZ* reporter
150 construct (Fig. 2A, B) in WT or strains lacking combinations of *lexA*, *higBA* or *higX*. Promoter
151 activity was unaffected by *higX* deletion in the WT or in Δ*higBA* backgrounds, but decreased in
152 Δ*lexA* Δ*higBAX* compared to Δ*lexA* Δ*higBA*, suggesting that HigX can activate the promoter
153 upstream of *higBA* when LexA and HigA are absent (Fig. 2B). We attempted to confirm this finding
154 by complementation with an overexpression construct containing *higX* under the control of the
155 vanillate-inducible promoter (pMT335-*higX*). However, we could not transform the Δ*lexA* Δ*higBA*
156 strain with this plasmid, suggesting that its increased level of *higX* expression is sufficiently toxic to
157 make the cells intolerant of transformation with a multi-copy plasmid containing *higX*, even in the
158 absence of inducer. Expression of *higX* from this plasmid in WT, Δ*lexA* or Δ*higBA* strains
159 containing the P_{higBA}-*lacZ* transcriptional reporter had a weak inhibitory effect on promoter activity,
160 which was only statistically significant in the Δ*higBA* background (Fig. 2C). Therefore, *higX* can
161 activate or repress the promoter upstream of *higBA*, dependent on which other regulators are
162 present, but its regulatory activity is weaker at this locus than that of LexA or HigA.

163 The different levels of mRNA expression for *higB* and *higX* observed by qRT-PCR (Fig. 1C) were
164 suggestive of regulation of the two transcripts by separate promoters, consistent with previous
165 genome-wide transcriptional profiling which identified independent primary transcriptional start
166 sites for *higBA* and *higX* (25), at genome positions 3281528 and 3280865 respectively. We
167 therefore constructed translational beta-galactosidase fusions of the regions immediately upstream
168 of *higB* and *higX* (including the first few codons of each of the genes) to *lacZ*, such that the *higB*
169 and *higX* reporter fusions should employ the native transcription start sites,. Surprisingly, the
170 translational fusion P_{higB}-*higB::lacZ* did not exhibit the same pattern of activity as the transcriptional
171 reporter (Fig. 2D, compare to 2B). For the translational reporter, the basal activity in WT, Δ*higBA*,
172 Δ*higBAX* or Δ*higX* strains was almost undetectable and high promoter activity was only observed

173 in the three strains lacking *lexA*, in contrast to the transcriptional reporter where basal expression
174 appeared high and the fold increase in the Δ*lexA* mutant strains was much less pronounced.
175 Conversely, the activity of the translational reporter for *higX* expression was much weaker (Fig 2E).
176 It was slightly LexA-dependent, but much less so than the promoter of *higB.* We conclude that *higX*
177 is primarily regulated by the strictly LexA-dependent promoter upstream of *higB*, despite having an
178 independent transcription start site, and that the different mRNA levels observed for *higB* vs. *higX*
179 (Fig. 1C) are due to other factors, for example processing or different stability. Moreover, the
180 strikingly low basal level of P_{higB}-*higB::lacZ* activity, relative to the transcriptional *lacZ* fusion of the
181 same region, is suggestive of an unknown post-transcriptional negative regulator of *higBA*.

182

183 ## HigX is a membrane-associated transcription factor

184 It was previously noted in a bioinformatic study of LytTR-family transcription factors (23) that all
185 members of this family in the *Caulobacter crescentus* genome, including *higX*, are likely to encode
186 transmembrane proteins. Bioinformatic prediction suggested that HigX contains four
187 transmembrane helices N-terminal to the LytTR DNA binding domain, with the transmembrane and
188 DNA-binding domains separated by a short low-complexity region (LCR) (Fig. 3A, S1A). The four
189 helices are predicted to form a tightly packed bundle with no apparent periplasmic domain (Fig.
190 S1B). To investigate whether the transmembrane domain was required for DNA binding activity,
191 we constructed another overexpression plasmid where the *higX* gene was truncated to convert
192 amino acid 133 (Val) to a new start codon, creating the *higX*-noTM variant containing only the LCR
193 and the LytTR domain. We expressed this alongside the full-length *higX* overexpression plasmid
194 and compared HigX abundance by western blotting using a custom polyclonal antibody to HigX
195 alongside cell extracts containing pMT335 empty vector and NA1000 without any plasmid as
196 control. It was only possible to detect HigX protein in the pMT335-*higX* overexpression strain,
197 showing that while the antibody can detect HigX, the native level of this protein is very low (Fig. 3B,
198 left). We could not detect the truncated HigX protein from the pMT335-*higX*-noTM overexpression

199 strain, suggesting that it may be unstable. Comparing the *Caulobacter* western blot results to cell
200 extracts of *E. coli* Rosetta cells containing pET28a-*higX* or pET28a-*higX*-noTM constructs intended
201 for protein purification, we observed that both the full-length and truncated proteins could be
202 detected in *E. coli* with our HigX polyclonal antibody (Fig. 3B, right). Therefore, although the
203 truncated version of HigX is not intrinsically unstable, it cannot be maintained in *Caulobacter* in the
204 absence of the TM domain.

205 To investigate whether HigX is localized to the membrane in living cells, we constructed C-terminal
206 GFP fusions to full length HigX and to the truncated HigX-noTM allele lacking the transmembrane
207 helices. Since the native level of HigX expression was so low, these were created as plasmid-
208 borne constructs under control of the vanillate-inducible promoter in order to have sufficient
209 expression to detect GFP fluorescence. Fluorescence microscopy showed that full length HigX
210 localizes uniformly around the cell periphery in both WT and filamentous cells (Fig. 3C), indicating
211 that normal cell division is not required for HigX subcellular localisation. No fluorescence was
212 observed in cells carrying the truncated HigX-noTM-GFP fusion protein, and overexpression of the
213 truncated HigX-noTM protein (without GFP fusion) had no effect on activity of the P_{higBA}-*lacZ*
214 transcriptional reporter (Fig. 3D), confirming that the transmembrane domain is essential for
215 stability and/or activity of HigX in the cell.

216 In order to detect the HigX native expression levels in WT and mutant strains, we employed
217 quantitative mass spectrometry. Protein extracts were prepared from WT, Δ*higBA*, Δ*higX*, Δ*lexA*,
218 and Δ*lexA* Δ*higBA* strains, with separation of the soluble (cytoplasmic) proteins from the insoluble
219 (membrane-associated) proteins before trypsinization and isotope labeling. A total of 1332
220 membrane-associated proteins were detected with two or more peptides, including HigX. No HigX
221 peptides were detected in the soluble fraction, indicating that the fluorescence observed at the cell
222 periphery in Fig 3C is due to membrane localisation. The abundance of HigX peptides was not
223 significantly changed between WT and Δ*higBA*, strongly depleted in Δ*higX* and enriched in both

224 Δ*lexA* and Δ*lexA* Δ*higBA* strains by 30-40% (Fig. 3E, Supplementary Table S1), consistent with the
225 trend observed in the translational reporter experiments (Fig. 2).
226

227 ## HigX acts independently of the toxin-antitoxin system HigBA

228 To test our hypothesis that overproduction of HigX was responsible for ciprofloxacin sensitivity in
229 Δ*lexA*, we expressed it *in tran*s from the vanillate-inducible promoter using pMT335-*higX* in WT,
230 Δ*lexA* and Δ*lexA* Δ*higB*. We found that *higX* overexpression had no effect on cell viability
231 compared to the empty vector control on normal media. However, on ciprofloxacin, *higX*
232 overexpression reduced viability of the Δ*lexA* strain compared to the empty vector. Strikingly, the
233 *higX* overexpression plasmid also reversed the improvement in ciprofloxacin resistance seen in the
234 Δ*lexA* Δ*higB* strain relative to empty vector (Fig. 4A). In addition to confirming that *higX*
235 overexpression was responsible for the ciprofloxacin sensitivity phenotype, this result also
236 indicated that HigX does not act solely through regulation of the TA system promoter, since the
237 phenotype was clearly visible in the absence of the HigB toxin. In support of the independence of
238 HigX from HigBA, we also observed an improvement of ciprofloxacin resistance in a Δ*lexA* Δ*higX*
239 double mutant relative to ΔlexA, where both of these strains have the *higBA* TA system genes
240 intact (Fig. 4B). This result demonstrates that the increased abundance of HigX seen in the Δ*lexA*
241 single mutant strain (Fig. 3D) contributes to its ciprofloxacin sensitivity in addition to (and
242 independently of) the overexpression of HigB.
243

244 ## HigX preferentially binds cell envelope, transport, and metabolism-associated genes

245 To assess the DNA binding capability of HigX, we performed chromatin immunoprecipitation
246 sequencing (ChIP-Seq) on wild type and Δ*lexA* strains using our polyclonal antibody to HigX.
247 Using the “MACS2 callpeak” program, we identified 596 significantly enriched peaks in the wild-
248 type strain (Supplementary Dataset S1). In contrast, peak calling for the Δ*lexA* strain revealed
249 genome-wide depletion of the enriched peaks, with 413 peaks identified with significant

250 enrichment, but with enrichment signal values uniformly lower than in WT (Fig 5A). Therefore, the
251 DNA-binding and thus regulatory function of HigX is strongly reduced upon deletion of *lexA*,
252 despite the 40% upregulation of HigX peptide abundance (Fig 3E). Significant peaks in the WT
253 strain were further filtered through a 95% threshold based on their signal value (≥ 3.22), resulting in
254 30 significant peaks that corresponded to the top 5% of the dataset. The highest of these peaks
255 was located between CCNA_03217 (a TetR-family transcriptional regulator) and CCNA_03218
256 (periplasmic multidrug efflux lipoprotein precursor), with the summit being closest to CCNA_03218
257 (Fig 5B).

258 To determine the overall function of HigX target genes and provide a holistic view of its potential
259 regulatory role, we extracted the summit locations of all 596 peaks and mapped them to the
260 nearest genes, followed by COG (Clusters of Orthologous Groups) annotation and functional
261 classification. From this, we observed that most peaks were associated with the following COG
262 categories, listed from most to least abundant: M, C, T, P, K, and J (Fig. 5C). However, when we
263 focused on the top 30 significant peaks (signal value ≥ 3.22), genes associated with carbohydrate
264 transport and metabolism (G) became the most prominent, while most of the previously dominant
265 categories (M, C, T, P, and K) remained to a lesser extent. In contrast, genes associated with
266 translation, ribosomal structure, and biogenesis (J) were no longer represented. This COG
267 distribution suggests that, for the 5% highest confidence ChIP peaks, HigX preferentially targets
268 genes associated with membrane, transport, and metabolism-related functions.

269 To further characterize the DNA-binding specificity of HigX, we performed a motif discovery
270 analysis by utilizing the summits of the 30 significant (top 5%) ChIP-seq peaks in conjunction with
271 MEME-ChIP. This analysis identified a significantly enriched 19-bp motif (E-value = 1.4×10^{-23})
272 present in 13 of the 30 submitted sequences, with a strong central enrichment, which indicates that
273 this motif likely represents the direct binding site of HigX (Fig. 5D). The motif is characterized by an
274 8-bp imperfect inverted repeat, with the left half spanning positions 4–11 (ATGTTASC) and the

275 right half spanning positions 12–19 (GSTACCAT), with no intervening spacer and a single
276 mismatch between the repeat halves.

277 Thus far, we had only investigated ciprofloxacin sensitivity of the Δ*lexA* strain and derivatives.
278 However, the ChIP-Seq analysis suggested that the dysregulation of HigX in the Δ*lexA* strain,
279 either at the level of overproduction of the protein or failure to bind the target genes, may also lead
280 to cell envelope irregularity that could lead to sensitivity to cell envelope-targeting antibiotics. We
281 therefore tested the ability of the Δ*lexA* and Δ*lexA* Δ*higX* strains to grow on cephalexin, which
282 targets septal peptidoglycan synthesis. The Δ*lexA* strain was sensitized to cephalexin relative to
283 WT, and cephalexin resistance was restored in the Δ*lexA* Δ*higX* double mutant (Fig. 5E).
284 Therefore, even though HigX production is under SOS control, its downstream effects in the cell
285 are more likely to be involved with cell envelope maintenance than with the SOS response.

286 Suppressor mutations in cell envelope-related genes improve ΔlexA ΔhigBA ciprofloxacin 287 resistance

288 To identify possible downstream effectors of HigX responsible for the overexpression phenotype,
289 we designed parallel forward genetic screening strategies to take advantage of (1) the Δ*lexA*
290 Δ*higBA* strain's sensitivity to ciprofloxacin and (2) its intolerance of transformation with the
291 pMT335-*higX* plasmid (Fig 6A). We constructed a pooled library of random *himar1* transposon (Tn)
292 mutants in the Δ*lexA* Δ*higBA* background in order to select for (1) ciprofloxacin-resistant Tn
293 mutants and (2) Tn mutants which can be stably transformed with pMT335-*higX*, using the Δ*lexA*
294 Δ*higBA* strain in preference to the Δ*lexA* strain in order to avoid selection of phenotypes due to the
295 HigB toxin. The first screen was performed by passage of the mutant pool through medium
296 containing 1 µg/ml ciprofloxacin, followed by selection of ciprofloxacin-resistant single colonies.
297 The second was performed by preparation of electrocompetent cells from a culture of the pooled
298 library, electroporation with pMT335-higX and plating on medium containing gentamicin and
299 vanillate (to select for the plasmid antibiotic resistance marker and to induce higX overexpression,
300 respectively). Such mutants should have Tn insertions in loci which suppress the HigX-mediated
301 phenotypes.

302 From our Tn mutant library of approximately 25’000 clones, we were able to obtain four stable Tn
303 mutants where we could confirm the desired phenotypes by re-plating on selective media
304 (ciprofloxacin, or gentamicin + vanillate) followed by backcrossing of the transposon mutations into
305 Δ*lexA* Δ*higBA* cells which had not been through the mutagenesis or selection procedure. All four
306 suppressor mutations were in or near genes associated with cell envelope-related functions (Fig.
307 6B). The two Tn mutants obtained from the ciprofloxacin resistance screen both had a Tn insertion
308 in or near CCNA_03248, encoding an uncharacterized TonB-dependent receptor. One insertion
309 was found within the coding sequence of CCNA_03248, while the other was in an intergenic region
310 218 bp upstream of the CCNA_03248 start codon. Notably, the Tn insertion site in the intergenic
311 region, at 3415650, is only 188 bp away from the peak summit of one of the significant (although
312 not top 5%) HigX binding sites, at 3415838, suggesting that this gene is a direct HigX target (Fig
313 6C). The two Tn mutants obtained from the pMT335-*higX* tolerance screen had Tn mutations in
314 CCNA_00669, encoding a lipopolysaccharide biosynthesis protein, and approximately 100 bp
315 upstream of the peptidoglycan amidase gene *amiC*. However, the two mutants obtained from the
316 pMT335-*higX* tolerance screen were also ciprofloxacin-resistant (Fig. 6D), and the mutants
317 obtained from the ciprofloxacin resistance screen could be transformed with pMT335-*higX*,
318 demonstrating that even if the genetic screens were not saturated, the selection strategies have
319 succeeded in isolating suppressor mutants with convergent phenotypes.

320 Taken together, these data support a model where overproduction of HigX in a Δ*lexA* background,
321 either from endogenous overproduction in Δ*lexA* strains or *in trans* from pMT335-*higX*, leads to
322 destabilization of the cell envelope. Since *higX* deletion protected the Δ*lexA* strain against Cipro
323 and cephalexin sensitivity even though HigX did not bind its target genes properly in the Δ*lexA*
324 mutant, the phenotype cannot be due to changes in HigX-dependent gene regulation but could be
325 a property of simply having too much HigX protein in the cell membrane, or having the protein
326 present but nonfunctional. We infer that our suppressor Tn mutants counteract the destabilizing
327 effect of HigX on the cell envelope, either directly or indirectly.

328

329 ## *higX* is widespread among alpha-proteobacteria but synteny with *higBA* is not conserved

330 To investigate whether this unusual combination of TA system with adjacent but independent
331 transcription factor was conserved among other bacteria, we evaluated the genomic conservation
332 of this locus using the FlaGs software (26) with the *Caulobacter crescentus* NA1000 HigX protein
333 sequence as query and the limit of aligned genomes set to 99, of which 68 were successfully
334 aligned. We observed that *higX* is not unique to *Caulobacter* species but found in many other
335 alpha-proteobacteria as well. Within the *Caulobacter* genus, the flanking gene context of *higX* was
336 well conserved, immediately upstream of the master cell cycle regulator *ctrA.* Moreover, it was co-
337 conserved with a conserved uncharacterized gene, annotated as a putative hydrolase of the
338 COG4188 family in all except five of the more distantly related genomes, including in the non-
339 *Caulobacter* species which did not have their *higX* orthologue adjacent to *ctrA* (Fig. S2). However,
340 in the 68 aligned *higX*-proximal regions, only four of the genomes contained probable *higBA*
341 orthologues upstream of *higX*. Hence, *higX* is much more conserved in its genomic context in
342 alpha-proteobacteria than *higBA* is (although we do not exclude that the other bacteria may
343 encode *higBA* at a different site in the genome, since at least in the *Caulobacter* genus it is
344 conserved between species (27)) and *higX* is almost universally found adjacent to the
345 uncharacterized hydrolase gene.

346 While examining the alignments of Fig S2 we noted that the intergenic region between the putative
347 hydrolase and the *higB* gene appeared consistently larger than the intergenic region between the
348 putative hydrolase and the *higX* gene (in the majority of genomes which lacked *higBA*), suggesting
349 that some of the intergenic sequence may be associated exclusively with the *higBA* genes. We
350 therefore aligned the intergenic regions between the putative hydrolase gene and *hig(BA)X* from a
351 subset of 15 *Caulobacter* genomes, including NA1000 and the four others which contained *higBA*
352 upstream of *higX*, and observed a consistent breakpoint in the intergenic region where the
353 intergenic sequence stopped in the genomes lacking *higBA*, but continued in the genomes which

354 had *higBA* upstream of *higX*. (Fig. 7A). This breakpoint was at base 3281622 of the *Caulobacter*
355 *crescentus* NA1000 genome, relative to the start codons of the putative hydrolase at base 3281744
356 and *higB* at base 3281524. From this, we inferred that of this intergenic region, the 122 bp adjacent
357 to the putative hydrolase gene is universal to all the genomes, while the additional 98 bp of
358 intergenic sequence found only in the genomes of the strains possessing *higBA* is likely to be a
359 *higBA*-specific regulatory element. Notably, this additional sequence contained the high-affinity
360 LexA binding site that is responsible for the LexA-mediated repression of the *higBA* promoter.
361 Therefore, the LexA-mediated repression of *higX* under normal conditions and the overproduction
362 of HigX when this repression is released is likely unique to NA1000 and the other *Caulobacter*
363 *crescentus/vibrioides* strains which contain *higBA* and its LexA-dependent promoter immediately
364 upstream of *higX*. In all other *higX*-encoding alphaproteobacteria, we would instead anticipate *higX*
365 to be expressed in a LexA-independent manner.

366 In order to investigate whether *higBA* is a recent arrival in a minority of the *Caulobacter* genomes,
367 or whether it is an ancestral factor that has been lost from the majority of them, we employed
368 compositional analysis of relative synonymous codon usage (RSCU) and tetranucleotide
369 frequency. Using multivariate compositional analysis of these two parameters (Supplementary
370 Dataset S2), we detected a minor atypicality of *higX* in its codon usage (q = 0.0211), but no
371 significant difference in tetranucleotide composition (q = 0.805) relative to other coding sequences
372 of the genome. In contrast, *higB* and *higA* displayed significant compositional atypicality in their
373 RSCU (*higB*: q = 3.83 x 10^{-37}, *higA*: q = 5.25 x 10^{-7}) and tetranucleotide composition (*higB*: q = 9.46
374 x 10^{-187}, *higA:* q = 4.39 x 10^{-144}), compared to all CDS within the genome. This degree of deviation
375 from the rest of the genome is potentially indicative of horizontal gene transfer or, at the least,
376 evidence for a recent arrival (Fig. 7B+C). The small deviation in codon usage for *higX* is likely
377 biologically negligible, with an effect size of 1.08 (i.e., 8% above the 95% cutoff; Figure S3A). By
378 comparison, *higB* and *higA* exhibited larger effect sizes (RSCU: 2.34 and 1.39; tetranucleotide:
379 2.66 and 2.43; Figure S3A). Thus, *higBA* appear to be compositionally highly atypical, whereas

380 *higX* is compositionally typical relative to the rest of the genome. We conclude from this that the
381 presence of *higBA* at this locus is most likely due to an insertion event into a recent ancestor of the
382 NA1000 lab strain of *Caulobacter* and a few closely related species, while the presence of *higX*
383 alone at this locus is the "ancestral" state.

384 ## *higX* is ancestral but *higBA* is of likely foreign origin

385 To support the compositional bias analysis, we investigated if the compositional typicality of *higX*
386 and atypicality of *higBA* was reflected in their encoded proteins' phylogeny, as an indication of their
387 most likely origin. The 16S rRNA phylogenetic tree showed that all genera cluster into separate
388 clades, with the only exception being *Asticcacaulis excentricus* CB 48, whose placement is within
389 the *Brevundimonas* clade (Fig. S3B). Regarding the presence/absence heatmap, as expected,
390 HigX was found to be the most prevalent protein across the order, with 13 organisms containing it
391 in different combinations and 9 containing it as the sole protein. Interestingly, the prevalence of all
392 3 proteins was not limited to members of the *Caulobacter* genus. In fact, one member of
393 *Brevundimonas* contained all three proteins. However, it is important to note that this heatmap
394 does not account for the synteny of the genes encoding the proteins. Thus, it is possible that even
395 if an organism contains all three proteins, they are not within the same gene cluster or operon.
396 *higBA* could likely be positioned away from *higX* somewhere else on the genome.

397 The protein phylogenetic trees to be compared against the 16S rRNA phylogenetic tree were
398 generated by utilizing BLASTx with *higB, higA* or *higX* as queries. Hits (n =100) were filtered and
399 used for creating a presence/absence heatmap of each gene per organism and in different
400 combination classes (Fig S4). Occurrence of all three proteins was limited to members of the
401 *Caulobacter* genus (n = 5), closely matching results of the heatmap from the 16S rRNA
402 phylogenetic tree (Figure S3B). HigB and HigA co-occurring in the absence of HigX were only
403 found in one species out of the 100 used and the co-occurrence of HigA and HigX was limited to
404 the *Caulobacter* genus (n = 7). Interestingly, in the remaining combination classes, a stark contrast
405 was observed. The class for HigB as the sole protein (n = 41) contained no organisms within the

406 Caulobacterales order (Fig S4, S5). In fact, twelve of these were members of the *Enterobacter*
407 genus, which is part of Gammaproteobacteria, showing a significant discrepancy with the 16S
408 rRNA phylogenetic tree. A similar pattern was observed for the HigA-only class (n = 59), whose
409 members consisted of organisms outside Caulobacterales (Figure S4, S6). By comparison, the
410 HigX-only class (n = 56) displayed a phylogeny similar to the 16S rRNA phylogenetic tree, with
411 only two organisms coming from outside the Caulobacterales order (Figure S4, S7). Overall, the
412 results from the phylogenetic analysis strongly indicate that *higX* is both ancestral to and
413 phylogenetically consistent with the Caulobacterales lineage, whereas the phylogenies of *higB* and
414 *higA* are indicative of a foreign genetic origin, possibly enterobacterial in the case of *higB*.

415 Discussion

416 In this study, we identify HigX as the factor responsible for the unexpected and HigB-independent
417 ciprofloxacin sensitivity of the Δ*lexA* Δ*higBA* mutant. Although HigX appeared at first to be a third
418 component of the HigBA TA system, due to its close genetic proximity, annotation as transcription
419 factor and ability to weakly regulate the *higBAX* promoter, we found that it does not exert its effect
420 through the TA system. Instead, it acts independently at the level of the cell envelope where it is
421 physically located and for which it regulates some of the genes. Δ*lexA* mutant strains produce
422 higher levels of HigX due to the placement of the *higX* gene directly downstream of the strong
423 LexA-dependent promoter of *higBA* and the lack of LexA to repress it, but this is not reflected in
424 increased binding of HigX to its target promoters. HigX is incorporated into the cell membrane
425 through its N-terminal domain, and high levels of HigX sensitize Δ*lexA* cells, but not WT cells, to
426 ciprofloxacin and cephalexin. Forward genetic screening showed that toxicity of excessive HigX
427 production can be suppressed by cell envelope-related mutations, including of at least one HigX
428 target gene.

429 Our compositional bias and phylogenetic analysis of *higBAX* revealed that higX appears to be
430 ancestral and phylogenetically conserved with a strong match to the 16S rRNA phylogeny of
431 *Caulobacter*. In contrast, *higB* and *higA* were found to be atypical in both the compositional

432 parameters (RSCU and tetranucleotide) and their phylogeny, suggesting a foreign nature.
433 Unexpectedly, the phylogeny of HigB was very different compared to HigA. The genus
434 *Enterobacter* was prevalent in the HigB tree (n=13), thus indicating this genus as the most likely
435 origin of *higB.* However, the potential origin of *higA* is less clear, as its prevalence is less clustered
436 to a single genus like *higB* and it did not display the same bias towards enterobacterial
437 orthologues. Instead, its occurrence is highest among *Stenotrophomonas* (n=10), *Bradyrhizobium*
438 (n=7), and *Xanthomonas* (n=5). Therefore, the potential source of *higA* acquisition can be reduced
439 to these three genera, with *Stenotrophomonas* being the most likely candidate. Taken together,
440 these results reveal that the toxin and antitoxin are of different evolutionary lineages and were
441 most likely acquired separately, rather than together, as previously documented (reviewed in (9,
442 28)).

443 Our initial observation that led us to investigate *higX* was the ciprofloxacin sensitivity phenotype of
444 the Δ*lexA* mutant. This had initially seemed counter-intuitive, given that this strain has the SOS
445 response constitutively activated in defence against DNA damaging drugs. However, part of the
446 SOS response in *Caulobacter* is to inhibit cell division through the divisome inhibitor protein SidA
447 (29) leading to the production of highly filamentous cells. *Caulobacter crescentus* is very sensitive
448 to cell envelope stress relative to other Gram-negative bacteria (30) and it could be that extreme
449 cell elongation weakens the integrity of the cell envelope, providing easier access to the cytoplasm
450 for antibiotics and accounting for the ciprofloxacin sensitivity. Excessive incorporation of cell
451 envelope proteins into the membrane and periplasm has been shown to cause cell envelope stress
452 in elongated cells where the filamentation was caused by different factors than the SOS response
453 (20), showing that LexA is not required for this effect. We propose that cell elongation-dependent
454 weakening of the envelope could be the reason why HigX overexpression is toxic to Δ*lexA* cells,
455 while WT cells are unaffected.

456 It was striking that global DNA binding of HigX was decreased in the Δ*lexA* cells even though they
457 produced more HigX protein than WT cells did. We find it unlikely that the reduced DNA binding of

458 HigX in the Δ*lexA* mutant is due to a global dependence on LexA for HigX binding, because in
459 comparing our regulon of HigX to the previously established ChIP-Seq regulon of LexA (15) we
460 found only 13 shared peaks, none of which were in our top 5% 30 HigX peaks. This suggests that
461 access of HigX to its target promoters is the major limiting factor in the Δ*lexA* strain. Restriction of
462 the protein to the inner face of the membrane would not limit nucleoid access in WT cells, because
463 the chromosomal DNA in *Caulobacter* does not condense but fills the whole cell during the normal
464 replication cycle (31). However, in filamentous cells, the DNA content is variable and depends on
465 whether chromosome replication has arrested or continued (32). If replication continues, the DNA
466 can continue to fill the cell volume, at least up to a point (33), but if it is inhibited then the
467 filamentous cell will have one or two nucleoids surrounded by DNA-free regions (34, 35). The
468 nucleoid arrangement in *Caulobacter* cells lacking LexA has not been imaged directly. However,
469 the DNA content of Δ*lexA* cells as measured by FACS is characteristic of replication arrest with
470 one or two chromosomes without over-replication (15), similar to cells with the SOS response
471 induced by mitomycin C (32). This would be insufficient, in most cases, to fill up the entire
472 cytoplasm of the highly filamentous Δ*lexA* cells. Therefore, even if more HigX is produced in Δ*lexA*
473 cells, some of the available membrane surface into which it can be inserted could be away from
474 the nucleoid, sequestering the protein away from the DNA and explaining the globally reduced
475 binding that we observe. Removal of HigX from its membrane localization does not improve DNA
476 access, since in our experiments with the truncated HigX lacking the four TM helices, we saw
477 neither gene regulation activity nor GFP fluorescence suggesting that the TM helix bundle is
478 required for the protein's stability. Together, these data support a model where correct HigX
479 regulatory activity can only happen with membrane-localised WT protein in normal shaped cells,
480 while activity is lost in elongated cells or if the HigX TM domain is missing (Fig 8). It will be
481 interesting to investigate whether HigX-dependent gene regulation is affected in cells that are
482 filamentous for other reasons (independent of LexA) in order to test this hypothesis, as this would
483 be more representative of HigX-dependent gene regulation in species that do not have the *higBA*
484 TA system genes and their LexA box immediately upstream.

485 Analysis of the regulon of HigX suggests that its cell membrane localisation may be linked to its
486 regulation of processes that happen there. Indeed, the highest peak that we observed was
487 associated with a periplasmic multidrug efflux lipoprotein precursor gene (CCNA_03218) (Fig 5B),
488 similar to the AcrA component of AcrAB-NodT family multidrug efflux pumps. The COG analysis of
489 the 5% top peaks had a noticeable representation of genes associated with transport of
490 carbohydrates, transport of inorganic ions, energy production/conversion and cell envelope or
491 membrane biogenesis (Fig 5C). We have not yet observed any phenotype linked to loss of HigX in
492 WT cells grown under lab conditions. However, its role may be more important for envelope
493 maintenance under stress conditions. The high level of evolutionary conservation of HigX across
494 the Caulobacterales order suggests that its presence is generally beneficial, even if currently
495 mysterious.

496 HigX's transmembrane conformation is unusual for a LytTR family protein. The majority of these
497 transcription factors are cytoplasmic and regulate extracellular processes such as competence,
498 alginate production, expression of virulence factors and bacteriocins (23). However, little is known
499 about how they are regulated themselves. In the original bioinformatic study which characterized
500 the LytTR transcription factors, it was noted that all of the instances of this domain discovered in
501 alpha-proteobacteria were probable membrane proteins (23), but without apparent periplasmic
502 domains that could allow them to function as extracellular sensors in the same way as the
503 membrane-bound transcription factors of *Vibrio cholerae* (36). Instead, their domain structure is
504 more similar to the enterococcal bacitracin-sensing response regulator BcrR, which is permanently
505 anchored to the inner membrane by a 4 helix transmembrane domain that senses bacitracin
506 directly and stimulates transcription of target genes by the DNA-binding domain (37). More recent
507 studies have identified a LytTR sub-family where the transcription factor is negatively regulated by
508 a separate membrane protein, designated "LytTR regulatory systems" (LRS). First identified in
509 *Streptococcus mutans* (38, 39), LRS are particularly abundant in the Firmicutes but also found in
510 some actinobacteria and a few gamma-, beta- and epsilon-proteobacteria (40). In LRS the LytTR

511 protein is consistently encoded upstream of the membrane protein, which usually consists of three
512 or four transmembrane alpha-helices and no apparent periplasmic domain, and the membrane
513 protein negatively regulates the transcription factor through membrane sequestration preventing it
514 from activating its target genes (41). The similarity of the topology of LRS membrane proteins to
515 the N-terminus of HigX (and the other Caulobacter LytTR proteins) is suggestive of the alpha-
516 proteobacteria having developed a new family of “fused LRS” where the transmembrane domain
517 and the DNA binding domain are in the same protein. However, the regulatory influence of the
518 transmembrane domain on the DNA binding domain would have to be positive rather than
519 negative, since we observe that full length HigX can carry out promoter regulation while the HigX
520 DNA binding domain without the transmembrane domain cannot (Fig. 3D), similarly to BcrR where
521 the DNA binding domain has no affinity for DNA without the transmembrane domain (37). A recent
522 computational study has revealed that transmembrane transcription factors are widely prevalent
523 throughout bacterial and archaeal taxonomic groups and may use the biophysical state of the
524 membrane as a signaling input to regulate gene expression (42), which could explain the
525 dependence that we see on the presence of the transmembrane domain for HigX.

526 In summary, we have uncovered a role for the first of this class of transmembrane transcription
527 factors from the alpha-proteobacteria to be characterized, and shown that cell filamentation
528 through loss of *lexA* negatively affects the ability of HigX to bind its target genes. In addition to
529 identifying a new type of cell envelope regulatory factor in *Caulobacter*, our findings also indicate
530 that TA system incorporation into a bacterial genome can cause alternative downstream
531 phenotypes that do not depend on the function of the TA system itself, but on the regulatory
532 element(s) that it brings along and the genomic context into which it arrives.

533

534 # Methods

535 ## General growth conditions

536 *Caulobacter crescentus* strains were routinely grown in peptone-yeast extract (PYE) medium at
537 30°C and *E. coli* strains in LB at 37°C. Antibiotics were used at the following concentrations;
538 tetracycline at 1 µg/ml for *Caulobacter* and 10 µg/ml for *E. coli*, gentamicin at 1 µg/ml
539 for *Caulobacter* and 10 µg/ml for *E. coli*, nalidixic acid at 20 µg/ml for *Caulobacter* and kanamycin
540 at 20 µg/ml (solid media) or 5 µg/ml (liquid media) for *Caulobacter* and 20 µg/ml for *E.*
541 *coli*. Ciprofloxacin was prepared as 20 mg/ml stock solution in 0.1 M HCl and in all experiments
542 involving ciprofloxacin, an equivalent volume of 0.1 M HCl was added to the control cultures or
543 plates. Vanillate stock solution was prepared at 50 mM stock solution (adjusted to pH 8.0 with
544 NaOH) and used at 50 or 100 µM as indicated in the figure legends.

545 ## Strain and plasmid construction

546 DNA fragments for cloning were PCR-amplified with Phusion DNA polymerase (Thermo Fisher
547 Scientific) from stationary phase cultures of wild type (WT) *Caulobacter crescentus*, using PCR
548 primers listed in Supplementary Table S2. Products were purified by agarose gel electrophoresis.
549 Cloning of the correct region was confirmed by sequencing and plasmid stocks were maintained
550 in *E. coli* EC100 or TOP10. Plasmids used in this work are listed in Supplementary Table
551 S3. Replicating plasmids (pMT335 (43), pJC327 (44) and plac290 derivatives) were transferred
552 into *Caulobacter* strains by electroporation while suicide plasmids for generation of deletion
553 mutants (pNPTS138 derivatives) and transposon mutants (pHPV414 (45)) were transferred by
554 conjugation from *E. coli* S17-1 *λpir* (46). After integration of suicide vectors by recombination
555 through one of the homologous flanking regions, secondary recombination events were induced by
556 counterselection on PYE agar containing 3% sucrose and mutants carrying resulting in-frame
557 deletions were screened for by PCR. Double mutants were made by introducing
558 the Δ*higX* or Δ*higBAX* alleles into the Δ*lexA* mutant strain. Generalised transductions with
559 bacteriophage ΦCr30 were performed as previously described (47). *C. crescentus* strain numbers

560 and genotypes are listed in Supplementary Table S4. pET28a derivatives containing WT or
561 truncated HigX fused to an N-terminal His-tag were expressed in *E. coli* Rosetta(DE3) (Novagen).

562 Efficiency of plating assays

563 Resistance to cephalexin and ciprofloxacin was assessed by dilution spot plating. Cultures of
564 strains to be tested were grown overnight to stationary phase, then inoculated into new medium to
565 grow to mid-exponential phase. Culture density was measured, normalised to the OD600 of the
566 least dense culture (OD600=0.5 or less), serially diluted in PYE to 10^{-6} and 5 µl spotted onto plates
567 containing PYE medium with sub-inhibitory concentrations of cephalexin (5 µg/ml) or ciprofloxacin
568 (1 µg/ml). For *higX* overexpression experiments, the plates additionally contained gentamicin in
569 order to maintain selection on the plasmid, and all plates contained vanillate (50 µM) to induce
570 overexpression of *higX*. Plates were imaged after 3 days growth at 30°C. Images are
571 representative of at least three independent biological replicates.

572 Beta-galactosidase assays

573 β-galactosidase assays were performed on strains carrying low copy plasmid-borne transcriptional
574 or translational fusions of the promoters of interest to l*acZ*. Cultures were grown to early
575 exponential phase (OD_{600} = 0.1 – 0.4) with exposure to ciprofloxacin or vanillate as described in
576 the main text or figure legends, followed by β-galactosidase assays using the method of
577 Miller (35) on three independent biological replicates.

578 RNA extraction and quantitative RT-PCR

579 RNA was extracted from 4 ml mid-exponential phase cultures which were treated with 2500 U
580 Ready-Lyse (Bionordika) and homogenized using QiaShredder columns, prior to RNA extraction
581 with the RNEasy Mini Kit (Qiagen) according to the manufacturers' instructions, including on-
582 column DNase digestion. RNA quality was assessed by agarose gel electrophoresis and
583 concentration was measured in a Nanodrop spectrophotometer. cDNA was prepared using
584 the SuperScript IV Reverse Transcriptase Kit (Thermo Fisher) according to the manufacturers'
585 instructions, on 400 ng RNA template using random hexamer primers. Quantitative RT-PCR was
586 performed in technical and biological triplicates on a 96-well LightCycler real-time PCR system

587 (Roche) using SYBR Green (Roche). The *higB* transcript was amplified with
588 primers higB_qrt_fwd and higB_qrt_rev, the *higX* transcript was amplified with primers
589 CC_3036_qrt_fwd and CC_3036_qrt_rev, and the reference gene *rpoD* was amplified with
590 primers rpoDfow and rpoDrev. Quantification was by the standard curve method
591 and *higB* and *higX* transcript levels were normalized to *rpoD*.

592 ## Western blot and anti-HigX antibody

593 Custom polyclonal antibody to HigX for western blotting and ChIP-Seq was developed by Nordic
594 Biosite. Rabbits were immunized with the synthetic peptide (C-)LRMEDHYVRIRTEHGSRLE
595 corresponding to amino acids 178 to 196 of the HigX protein with cysteine conjugated at the N-
596 terminus. Antiserum was extracted from the rabbits and affinity purified on a Sepharose column
597 containing the immobilized synthetic peptide to obtain purified polyclonal antibody. Cell extracts for
598 western blotting were prepared by growing *Caulobacter* cultures in PYE (containing 50 μM
599 vanillate for strains containing pMT335 derivatives), or *E. coli* Rosetta(DE3) cultures in LB with 0.1
600 mM IPTG, to mid-exponential phase, normalizing to OD600 = 0.5, centrifuging and resuspending in
601 100 μl SDS-PAGE loading buffer. Extracts were run on a 16% SDS-PAGE gel alongside
602 PageRuler prestained markers (Thermo Fisher). Proteins were transferred to PVDF membranes
603 and blocked by incubation in TBS containing 5% dried skim milk. HigX protein was detected by
604 incubation with primary antibody diluted 1/5000 in TBS with 2% skim milk at 4°C overnight,
605 secondary antibody diluted 1/4000 in TBS with 2% skim milk at 4°C for one hour, and HRP
606 substrate at room temperature for one minute. Between incubations, membranes were washed 2 x
607 5 minutes then 1 x 15 minutes in TBS.

608 ## Microscopy

609 Cultures for imaging were grown to mid-exponential phase with 50 μM vanillate to induce HigX-
610 GFP expression and immobilized on 1% agarose (in water) microscope slides. Phase-contrast and
611 GFP fluorescence images were obtained with an inverted Olympus IX83 microscope equipped with
612 a 100x/1.46 oil objective and a Photometrics Prime scientific complementary metal-oxide-

613 semiconductor (sCOMS) camera. GFP images were taken before phase-contrast images to
614 minimize bleaching. Images are representative of three independent biological replicates.

615 ## Quantitative mass spectrometry

616 Cultures for mass spectrometry were grown to mid-exponential phase, harvested by centrifugation
617 and cell pellets were immediately frozen in liquid nitrogen. Cells were sonicated in ice-cold 100 mM
618 Na_2CO_3 containing cOmplete protease inhibitor and PhosSTOP phosphatase inhibitor (Sigma) for
619 2x20 sec at 60% amplitude on ice using a probe sonicator. After sonication the samples were
620 incubated at 4 °C for 1h with rotation. After incubation, the samples were ultracentrifuged at
621 100.000g for 90 min using a Hitachi Micro ultracentrifuge (CS 150 NX). After ultracentrifugation,
622 the supernatants (soluble protein fraction) were transferred to another tube and the membrane
623 pellets were gently washed with 100µL 50 mM TEAB, pH 8.5. The membrane pellets were
624 resolubilized in 5% sodium deoxycholate (SDC) in 50 mM HEPES buffer, pH 8.5, by probe
625 sonication (1x20 sec at 20% amplitude). After sonication, the samples were centrifuged at 20.000g
626 for 10 min, the supernatants were transferred to new tubes and the protein concentrations were
627 measured by Nanodrop (Implen Nanophotometer N60). The membrane protein samples were
628 reduced and alkylated using 5 mM DTT for 30 min and 10 mM iodoacetamide for 30 min,
629 respectively. After alkylation, trypsin was added (5%) and the samples were incubated at 37 °C
630 over-night. After incubation, additional trypsin (1%) was added and incubated at 37 °C for 1 hour.

631 A total of 25 µg of peptides from all conditions were labeled with Tandem Mass Tag (TMT) pro 18
632 plex (Thermo Fisher Scientific) according to the manufacturer's protocol. The TMT labeling was
633 performed as following: NA1000 (TMT 126, 127N and 127C); Δ*higBA* (TMT 128N, 128C and
634 129N); Δ*higX* (TMT 129C, 130N and 130C); Δ*lexA* (TMT 131N, 131C and 132N); Δ*lexA* Δ*higBA*
635 (TMT 132C, 133N and 133C). After labeling, all samples were combined into one sample and the
636 SDC was precipitated by adding formic acid to 2% followed by centrifugation at 20.000g for 20 min.
637 The supernatant was transferred to a new Eppendorf tube and dried by vacuum centrifugation. The
638 dried TMT labeled peptides were desalted using Poros Oligo R3 Reversed Phase (RP) material

639 and subsequently fractionated using high pH RP fractionation into 12 concatenated fractions as
640 described previously (PMID: 35240313). Each fraction was dried and resolubilized in 10 µL 0.1%
641 formic acid prior to liquid chromatography tandem mass spectrometry (LC-MS/MS).

642 An aliquot of each peptide fraction was loaded onto a 20 cm analytical column (100 µm inner
643 diameter) packed with ReproSil – Pur C18 AQ 1.9 µm RP material using an EASY nanoLC system
644 coupled to an Orbitrap Eclipse Tribrid (Thermo Fisher Scientific). The peptides were eluted with an
645 organic solvent gradient from 100% phase A (0.1% FA) to 22% phase B (95% ACN, 0.1% FA) for
646 100 min, then from 22% B to 40% B for 20 min before the column was washed with 95% B. The
647 flow rate was set to 300 nL/min during elution. The automatic gain control target value was $1.5x10^6$
648 ions in MS and a maximum fill time of 50 ms was used. Each MS scan was acquired at high-
649 resolution (120,000 full width half maximum (FWHM) at m/z 200) in the Orbitrap with a mass range
650 of 350-1500 Da. The instrument was set to select as many precursor ions as possible in 3 sec
651 between the MS scans. Peptide ions were selected from the MS for higher energy collision-
652 induced dissociation (HCD) fragmentation (collision energy: 34%). Fragment ions were detected in
653 the orbitrap at high resolution (50,000 FWHM) for a target value of $1,5x10^5$ ions and a maximum
654 injection time of 150 ms using an isolation window of 0.7 Da and a dynamic exclusion of 20 sec. All
655 raw data were viewed in Xcalibur v3.0 (Thermo Fisher Scientific).

656 All LC-MS/MS raw data files were searched in Proteome Discoverer (PD) version 2.5.0.400
657 (Thermo Fisher Scientific) using the SEQUEST HT search algorithm against the *Caulobacter*
658 *crescentus* (strain NA1000 / CB15N) OX=565050 protein FASTA database. The searches had the
659 following criteria: enzyme, trypsin; maximum missed cleavages, 2; fixed modifications, TMTpro (N-
660 terminal), TMTpro (K) and Carbamidomethyl (C).

661 The TMTpro reporter ion signals were quantified using S/N and they were normalized to the total
662 peptide S/N in the PD program. The in-built ANOVA test in PD was used to generate p-values for all
663 the proteins identified in the database searches with 1% FDR.

664 ## ChIP-Seq sample preparation and sequencing

665 Chromatin immunoprecipitation (ChIP) was performed essentially as described in Fumeaux et al
666 (48) with the following modifications. Cultures were grown to mid-exponential phase in 80 ml PYE
667 before formaldehyde crosslinking. Sonication was carried out in a Covaris ultrasonicator with the
668 following settings: temperature 6°C, duration 3600 seconds, peak power 75.0, duty % factor 10.0,
669 cycles per burst 200, average power 7.5, delay 60 seconds. All of the cleared sonicated lysate was
670 used for ChIP without taking an input sample out first. HigX-bound DNA was recovered by
671 immunoprecipitating with 20 µg purified anti-HigX antibody per sample, divided between two
672 Eppendorf tubes. After immune complex recovery, reversal of crosslinks and protease treatment,
673 DNA was recovered in 50 µl MilliQ water per Eppendorf and pooled into 100 µl, of which 40 µl was
674 used for sequencing. DNA was prepared for Illumina sequencing using the NEBNext UltraExpress
675 DNA library preparation kit (New England Biolabs) according to the manufacturer's instructions and
676 50 bp paired-end sequencing was carried out on a NovaSeq 6000 (Illumina). Details of the
677 sequence processing, alignment, quantification and data analysis are in the Supplementary
678 methods.

679 ## Transposon mutagenesis, forward genetic screening and insertion mapping

680 A pooled library of transposon mutants was constructed in the Δ*lexA* Δ*higBA* background by
681 performing five independent conjugations of the transposon carrier plasmid pHPV414 from *E. coli*
682 S17-1 *λpir* into the Δ*lexA* Δ*higBA* recipient strain. Transconjugant colonies were selected on PYE
683 plates with nalidixic acid and kanamycin after three days incubation at 30°C. Colony counting
684 indicated that the library consisted of > 25’000 independent clones. Colonies were pooled in PYE
685 and stored in aliquots at -80°C in 10% DMSO.

686 The ciprofloxacin resistance screen was performed by growing the pooled library to stationary
687 phase and diluting it into medium containing 1 µg/ml ciprofloxacin and 20 ug/ml kanamycin,
688 followed by plating on PYE plates containing 1ug/ml ciprofloxacin and 20 ug/ml kanamycin, and
689 incubation at 30°C for five days. 40 colonies were re-streaked on PYE plates containing 1 µg/ml
690 ciprofloxacin and 20 ug/ml kanamycin followed by incubation for 4 days to confirm growth.

691 The HigX overexpression tolerance screen was performed by growing the pooled library to
692 stationary phase, preparing electrocompetent cells and electroporating with pMT335-*higX*.
693 Plasmid-tolerating colonies were selected by plating electroporated cells on PYE plates containing
694 gentamicin and 50 μM vanillate. Colonies were re-streaked to new gentamicin/vanillate plates to
695 confirm stability of the phenotype.

696 Transposon insertion sites were mapped by plasmid rescue. Genomic DNA was extracted from the
697 ciprofloxacin-resistant or HigX-tolerant transposon mutants, partially digested with *Sau*IIIA and
698 ligated. Ligations were used to transform *E. coli* EC100D, in which the transposon can be
699 maintained as a replicating plasmid, and selected for kanamycin resistance. Plasmids were
700 extracted and sequenced with the transposon-specific himup2 primer across the junction between
701 the transposon insertion site and the flanking genomic DNA. To confirm specificity of the
702 transposon insertions for the observed phenotypes, the transposon insertions were back-crossed
703 into the Δ*lexA* Δ*higBA* strain by bacteriophage ΦCr30-mediated generalized transduction. The
704 resulting strains were tested for both ciprofloxacin resistance and tolerance of electroporation with
705 pMT335-*higX*.

706 Sequence alignment and analysis

707 The genomic context conservation of HigX orthologues was investigated with FlaGs (26).
708 Transmembrane segment prediction was performed with the DAS TM prediction program (49) and
709 the structure was modelled in Alphafold using default parameters (50). Multiple sequence
710 alignment of the region spanning *CCNA_03134* to *ctrA* was performed with MAFFT (51) (default
711 parameters) and visualized with Molecular Evolutionary Genetics Analysis version 11 (52) (MEGA
712 version 11.0.13). Details of compositional bias analysis, comparative genomics and phylogenetic
713 analysis of proteins and 16S RNA sequences are in the Supplementary Methods.

714 Statistical analysis

715 All numerical data are reported as mean of all biological replicates performed and error bars
716 indicate the standard deviation. Statistical significance was analysed by non-paired equal

variance 2-tailed Student's T test for simple pairwise comparisons between strains or treatment conditions and by a Dunnett's test in R (version 4.2.2) for multiple comparisons. Dunnett's test in R was carried out by setting the wild-type strain (NA1000) as a reference and comparing all other strains against it. * signifies $p < 0.05$, ** signifies $p < 0.01$ and *** signifies $p < 0.001$ throughout.

Acknowledgements

This work was supported by a grant from Independent Research Fund Denmark and start-up funding from the University of Southern Denmark, both to CLK. We are grateful to Asmus Cosmos Skovgaard for technical assistance. We thank Bert Ely, Gemma Atkinson, Nathan Fraikin and Ditlev Brodersen for helpful discussions and Vishnu Narayanan Madhavan for critical reading of the manuscript. Sequencing of DNA for ChIP-Seq was carried out at the Center for Functional Genomics and Tissue Plasticity, Functional Genomics & Metabolism Research Unit, University of Southern Denmark. The authors thank Ronni Nielsen for sequencing assistance.

Author contributions

CLK conceptualized and designed the study. KAB, NVH, KG, SN, LHH, LAJ, MRL and CLK performed experiments. MRL analysed the quantitative proteomics data. NVH and CLK analysed ChIP-Seq data and performed statistical analysis. KAB, KG, NVH, MRL and CLK wrote the paper.

Competing interests

The authors declare that no competing interests exist.

Data availability

739 The Fastq files containing the raw data from the ChIP-Seq experiments in WT and Δ*lexA* for HigX
740 genome binding have been deposited in GEO under the accession number GSE310922. All other
741 data is available within the paper or in its Supporting Information.

742 Figure legends

743 Figure 1. The higBA toxin-antitoxin system has a transcription factor closely associated 744 with it.

745 (A) Operon structure of *higBA* and location of the downstream gene *CCNA_03131* (*higX*). The
746 promoter upstream of *higBA* is negatively regulated by LexA and HigA. The *higB* and *higA* genes
747 are translationally coupled, with 7 bp overlap between the stop codon of *higB* and the start codon
748 of *higA*, while the *higX* start codon is 42 bp downstream of the *higA* stop codon. (B) Efficiency of
749 plating assay of WT *Caulobacter* (NA1000) and mutant strains lacking combinations of *lexA*, *higB*,
750 *higA* and/or *higX*, on 0.5 µg/ml ciprofloxacin or vehicle control. Images are representative of three
751 independent biological replicates. (C) Quantitative RT-PCR of mRNA levels of *higB* and *higX*,
752 normalized to the control transcript *rpoD*. Data was obtained from three independent biological
753 replicates.

754 Figure 2. Translational reporter constructs show that higB, higA and higX are 755 independently regulated.

756 (A) Construction of the transcriptional (red) or translational (green) reporter fusions to lacZ from
757 regions of the *higBAX* genomic locus. The transcription start sites in this region previously detected
758 by global mapping (25) are shown as red arrows. (B-C) Transcriptional beta-galactosidase reporter
759 assays in WT and mutant strains lacking combinations of *lexA*, *higB*, *higA* and/or *higX* (B) and WT,
760 Δ*lexA* and Δ*higBA* strains containing the empty vector pMT335 or the *higX* overexpression plasmid
761 pMT335-*higX*. Overexpression of *higX* was induced by 50 µM vanillate (C). (D-E) Translational
762 beta-galactosidase reporter assays in WT and mutant strains lacking combinations of *lexA*, *higB*,
763 *higA* and/or *higX* for a *lacZ* in-frame fusion to the *higB* upstream region and first ten codons of
764 HigB (D), and a *lacZ* in-frame fusion to the *higX* upstream region and first four codons of HigX (E).
765 A promoterless negative control of the translational fusion construct was tested in WT and had
766 undetectable beta-galactosidase activity (zero to two Miller units).

767 Figure 3. The N-terminal region of HigX localizes it to the cell periphery and is required for
768 higBA promoter regulatory activity.
769 (A) Predicted domain structure (from Uniprot) of HigX with transmembrane helices (TM1-4)
770 indicated in blue, low-complexity region (LCR) in green and the LytTR DNA-binding domain in
771 orange. The black pin indicates where in the *higX*-noTM construct, amino acid Val133 was
772 converted to a new Met start codon to create a truncated version consisting of the DNA binding
773 domain without any transmembrane helices. (B) Western blots of cell extracts of *Caulobacter* cells
774 expressing *higX* or *higX*-noTM in pMT335 with 50 μM vanillate induction (left) or E. coli Rosetta
775 expressing His6-HigX in pET28a with 0.1 mM IPTG induction (right), with the anti-HigX polyclonal
776 antibody. Solid arrows indicate the size of full-length HigX (28.2 kDa) and the dotted arow indicates
777 the size of HigX-noTM (14.6 kDa). (C) Phase-contrast and fluorescence microscopy of WT and
778 Δ*lexA* Δ*higX* expressing a HigX-GFP translational fusion from the vanillate-inducible promoter.
779 Scale bars indicate 2 μm. No GFP fluorescence was observed for cells carrying the pMT335 empty
780 vector. (D) Beta-galactosidase assay of the transcriptional P_{higBAX}-lacZ reporter in WT and Δ*higBA*
781 strains containing the empty vector pMT335, the full length *higX* overexpression plasmid pMT335-
782 *higX* or the truncated *higX* overexpression plasmid pMT335-*higX*-noTM. No statistically significant
783 difference was observed between the empty vector control and the *higX*-noTM overexpression
784 plasmid. (E) Relative abundances of HigX peptides in Δ*higBA*, Δ*higX*, Δ*lexA* and Δ*lexA* Δ*higBA*
785 membrane-enriched cell extracts detected by mass spectrometry and normalized to WT. Values
786 are the averages of three independent biological replicates. Peptide abundance values (averages),
787 CV% values (% coefficient of variation) and p values are in Supplementary Table S1. Note that
788 non-zero values for HigX peptides in the Δ*higX* strain are likely derived from the vestiges of the
789 start and end of the *higX* coding region that remain in place after the in-frame deletion, and/or low-
790 frequency detection of peptides derived from other proteins that coincidentally have the same
791 mass/charge ratio as HigX-derived peptides.

792 Figure 4. Overexpression of higX in trans causes ciprofloxacin sensitivity independently of
793 the higBA toxin-antitoxin system.
794 (A) Efficiency of plating assay of WT, Δ*lexA* and Δ*lexA* Δ*higB* containing empty vector pMT335 or
795 the *higX* overexpression plasmid pMT335-*higX*. All plates contained gentamicin and 50 μM
796 vanillate in addition to ciprofloxacin (0.5 μg/ml) or vehicle control. (B) Efficiency of plating assay of
797 WT, Δ*lexA* and Δ*lexA* Δ*higX* on ciprofloxacin (0.5 μg/ml) or vehicle control. Images are
798 representative of three independent biological replicates.

799 Figure 5. Genome-wide analysis of HigX DNA-binding and functional enrichment.
800 (A) ChIP-seq profiles of HigX in *Caulobacter* NA1000 wild-type (WT, blue) and Δ*lexA* (yellow)
801 strains, with the data plotted as reads per million (RPM) across the genome. (B) Zoom-in of the
802 highest peak in the dataset located between *CCNA_03217* and *CCNA_03218*, with a gene track
803 displaying the transcriptional orientation. The peak region is highlighted in red, and the summit
804 position is indicated by a red dashed line. (C) COG analysis of significant ChIP-seq peaks in the
805 WT strain. Blue bars represent all significant peaks identified by MACS2, while red bars indicate
806 peaks filtered by a signal value threshold (≥ 3.22). Two categories were omitted: “Function
807 unknown (S)” with 66 (blue) and 3 (red) counts, and “Unassigned (no COG)” with 177 (blue) and 9
808 (red) counts. (D) Sequence logo of the HigX binding motif identified through MEME-ChIP from the
809 peak summit regions of the filtered peaks from the WT (signal value ≥ 3.22). The motif consists of
810 an imperfect inverted repeat of 8-bp with no intervening spacer. The left half of repeat is located at
811 positions 4–11 (ATGTTASC) and the right half at positions 12–19 (GSTACCAT) with a single
812 mismatch between the repeat halves. (E) Efficiency of plating assay of WT, Δ*lexA* and Δ*lexA*
813 Δ*higX* on cephalexin (5 μg/ml) or vehicle control. Images are representative of three independent
814 biological replicates.

815

816 Figure 6. Forward genetic screening for suppressors of ΔlexA ΔhigBA ciprofloxacin
817 sensitivity reveals cell envelope-related genes.
818 (A) Schematic of the forward genetic screening protocol in the Δ*lexA* Δ*higBA* strain for
819 ciprofloxacin resistance (left) and pMT335-*higX* transformation tolerance (right). (B) Location of the

820 transposon insertions in the four verified suppressor mutants. The insertion sites at the
821 CCNA_03248 locus are at 3415650 (upstream) and 3417411 (inside CDS), the insertion site in the
822 CCNA_00669 gene is at 727111 and the insertion site upstream of the *amiC* gene is at 2097088.
823 (C) Zoom-in of the ChIP-Seq profiles of WT (blue) and Δ*lexA* (yellow) at the CCNA_03248 locus.
824 (D) Efficiency of plating assay of WT, Δ*lexA* Δ*higBA* and Δ*lexA* Δ*higBA* transduced with three of
825 the suppressor transposon mutations, on ciprofloxacin (0.5 µg/ml) or vehicle control. Images are
826 representative of three independent biological replicates.

827 Figure 7. HigX is broadly conserved in its genomic context while higBA is restricted to the
828 Caulobacter crescentus/vibrioides lineage.
829 (A) Alignment of the intergenic region upstream of *hig(BA)X* containing the breakpoint between
830 +*higBA* and -*higBA* strains. The DNA sequence shown corresponds to bases 3281574 to 3281632
831 of the NA1000 genome sequence. The LexA binding motif is shown in yellow. (B) Multivariate
832 compositional analysis of relative synonymous codon usage (RSCU) across all coding sequences
833 in *Caulobacter* NA1000 with individual CDSs represented as grey points and the 95 % confidence
834 intervals around the genomic centroid indicated as a dashed ellipse. The three genes of interest
835 are indicated as *higB* (orange), *higA* (blue) and *higX* (green). Below the PCA plot, density plots
836 display the genome-wide distributions of Mahalanobis distance (MD^2) under both standard two-
837 dimensional (PC1–PC2) and robust minimum covariance determinant (MCD) models (k = 35).
838 Empirical FDR < 0.05 cutoffs (Benjamini–Hochberg), are shown as black dotted lines and the MD^2
839 values for *higB*, *higA* and *higX* are indicated in their respective colors. (C) Multivariate
840 compositional analysis of tetranucleotide frequencies using the same approach as in (B). The
841 tetranucleotide frequency composition of each gene was normalized and projected into principal
842 component space, with the 95% confidence intervals around the genomic centroid indicated as a
843 dashed ellipse. Once again, *higB*, *higA*, and *higX* are shown in their respective colors, and the
844 density plots display the corresponding MD^2 distributions for both two-dimensional and robust MCD
845 models (*k* = 160) with FDR-based significance thresholds.

846 Figure 8. Model for the cell-shape dependent regulatory activity of HigX in Caulobacter.
847 HigX promoter binding is active in WT cells with native HigX protein, but not in filamentous Δ*lexA*
848 cells or WT shaped cells expressing HigX without its N-terminal transmembrane (TM) domain
849 which is likely unstable or inactive. The nucleoid is represented in blue and HigX in orange.
850 Resistance to ciprofloxacin and cephalexin is correlated with loss of HigX itself rather than loss of
851 HigX DNA-binding activity (? indicates that this has not been tested for HigX-noTM).

852 Supplementary Figure legends

853 Figure S1. Structure prediction of HigX as a transmembrane LytTR-family transcription
854 factor.
855 (A) Prediction of the transmembrane helix locations by DAS. (B) Model structure prediction of HigX
856 by Alphafold, showing the N-terminal domain as a tightly packed four-helix bundle and the C-
857 terminal domain with the typical LytTR DNA binding domain.

858 Figure S2. Extended FLaGs analysis of genomic context around HigX shows that it is
859 widely conserved with a divergent putative hydrolase enzyme across other alpha-
860 proteobacterial genera.
861 Output of FLaGs analysis using the results of a BLASTP search of HigX against known alpha-
862 proteobacterial genomes (the BLASTP query sequence of *Caulobacter crescentus* NA1000 HigX is
863 not included here, only the BLASTP output), with the limit of aligned genomic regions increased to
864 99, of which 68 were aligned. The number codes for selected proteins with annotated functions are
865 as follows: 1, uncharacterized putative hydrolase; 2, FliI; 3, CtrA; 4, FliJ; 5, LdpD; 22, HigA; 25,
866 HigB.

867 Figure S3. Effect size of the compositional bias and phylogenetic conservation of the
868 higBAX locus.
869 (A) Effect size analysis of *higB*, *higA*, and *higX* based on codon usage (RSCU) and tetranucleotide
870 frequency composition. Bars represent the square root of the Mahalanobis distance^2 ($\sqrt{MD^2}$)
871 relative to the 95% robust cutoff (MCD estimator), expressed as a fold over the threshold. The 95%
872 cutoff (effect size = 1) is indicated as a dashed horizontal line, meaning that values above this
873 indicate deviation from the genome-wide compositional background. (B) Phylogenetic tree of the
874 order Caulobacterales showing the distribution of the proteins HigB, HigA, and HigX. The

875 maximum-likelihood tree was constructed from 16S rRNA sequences of complete and reference
876 genomes (n = 24) retrieved from NCBI, serving as a phylogenetic standard for comparison. The
877 accompanying heatmap indicates the presence or absence of the three proteins across the same
878 genomes. Note that the heatmap does not account for gene synteny.

879 Figure S4. Distribution of HigB, HigA, and HigX homologs across bacteria
880 Presence–absence heatmap showing the occurrence of HigB, HigA, and HigX homologs across
881 bacterial genomes identified by BLASTX searches against the NCBI RefSeq protein database.
882 Each column indicates one of the three proteins, and each row corresponds to an organism with
883 both its scientific name and NCBI TaxID. Presence/absence (blue/grey) is indicated by the left
884 sidebar, and the right sidebar indicates protein combinations. Note that the heatmap does not
885 account for gene synteny.

886 Figure S5. Phylogeny of HigB homologs across bacteria
887 Phylogenetic tree of HigB homologs based on protein sequences retrieved from the top BLASTX
888 hits. Sequences were aligned with MAFFT (L-INS-i), followed by inference of the tree with IQ-
889 TREE using the maximum-likelihood method. The tree was midpoint-rooted for visualization, with
890 tip labels displaying organism names, which have been colored by genus. Bootstrap support
891 values (≥ 50) are displayed at internal nodes, and the scale bar indicates the number of amino-acid
892 substitutions per site. The phylogram in the upper left corner shows a condensed version of the
893 16S phylogenetic tree (Figure S4B), which acts as a phylogenetic standard for comparison.

894 Figure S6. Phylogeny of HigA homologs across bacteria
895 Phylogenetic tree of HigA homologs based on protein sequences retrieved from the top BLASTX
896 hits. Sequences were aligned with MAFFT (L-INS-i), followed by inference of the tree with IQ-
897 TREE using the maximum-likelihood method. The tree was midpoint-rooted for visualization, with
898 tip labels displaying organism names, which have been colored by genus. Bootstrap support
899 values (≥ 50) are displayed at internal nodes, and the scale bar indicates the number of amino-acid
900 substitutions per site. The phylogram in the upper left corner shows a condensed version of the
901 16S phylogenetic tree (Figure S4B), which acts as a phylogenetic standard for comparison.

902 Figure S7. Phylogeny of HigX homologs across bacteria
903 Phylogenetic tree of HigX homologs based on protein sequences retrieved from the top BLASTX
904 hits. Sequences were aligned with MAFFT (L-INS-i), followed by inference of the tree with IQ-
905 TREE using the maximum-likelihood method. The tree was midpoint-rooted for visualization, with
906 tip labels displaying organism names, which have been colored by genus. Bootstrap support
907 values (≥ 50) are displayed at internal nodes, and the scale bar indicates the number of amino-acid
908 substitutions per site. The phylogram in the upper left corner shows a condensed version of the
909 16S phylogenetic tree (full version in Figure S4B), which acts as a phylogenetic standard for
910 comparison.

911 References

912 1. Baharoglu Z, Mazel D. SOS, the formidable strategy of bacteria against aggressions.
913 FEMS Microbiology Reviews. 2014;38(6):1126-45.
914 2. Erill I, Campoy S, Barbé J. Aeons of distress: an evolutionary perspective on the
915 bacterial SOS response. FEMS Microbiology Reviews. 2007;31(6):637-56.
916 3. Chen Z, Yang H, Pavletich NP. Mechanism of homologous recombination from the
917 RecA–ssDNA/dsDNA structures. Nature. 2008;453(7194):489-94.
918 4. Kovačič L, Paulič N, Leonardi A, Hodnik V, Anderluh G, Podlesek Z, et al. Structural
919 insight into LexA–RecA* interaction. Nucleic Acids Research. 2013;41(21):9901-10.
920 5. Fernández de Henestrosa AR, Ogi T, Aoyagi S, Chafin D, Hayes JJ, Ohmori H,
921 Woodgate R. Identification of additional genes belonging to the LexA regulon in Escherichia coli.
922 Molecular Microbiology. 2000;35(6):1560-72.
923 6. Kamenšek S, Podlesek Z, Gillor O, Žgur-Bertok D. Genes regulated by the
924 Escherichia coli SOS repressor LexA exhibit heterogenous expression. BMC Microbiology.
925 2010;10(1):283.
926 7. Pandey DP, Gerdes K. Toxin-antitoxin loci are highly abundant in free-living but lost
927 from host-associated prokaryotes. Nucleic Acids Res. 2005;33(3):966-76.
928 8. Harms A, Brodersen DE, Mitarai N, Gerdes K. Toxins, Targets, and Triggers: An
929 Overview of Toxin-Antitoxin Biology. Molecular Cell. 2018;70(5):768-84.
930 9. Jurėnas D, Fraikin N, Goormaghtigh F, Van Melderen L. Biology and evolution of
931 bacterial toxin–antitoxin systems. Nature Reviews Microbiology. 2022;20(6):335-50.
932 10. Page R, Peti W. Toxin-antitoxin systems in bacterial growth arrest and persistence.
933 Nature Chemical Biology. 2016;12(4):208-14.
934 11. Ronneau S, Helaine S. Clarifying the Link between Toxin–Antitoxin Modules and
935 Bacterial Persistence. Journal of Molecular Biology. 2019;431(18):3462-71.
936 12. Christensen-Dalsgaard M, Jorgensen MG, Gerdes K. Three new RelE-homologous
937 mRNA interferases of Escherichia coli differentially induced by environmental stresses. Mol
938 Microbiol. 2010;75(2):333-48.
939 13. Dorr T, Vulic M, Lewis K. Ciprofloxacin causes persister formation by inducing the
940 TisB toxin in Escherichia coli. PLoS biology. 2010;8(2):e1000317.
941 14. Kawano M, Aravind L, Storz G. An antisense RNA controls synthesis of an SOS-
942 induced toxin evolved from an antitoxin. Mol Microbiol. 2007;64(3):738-54.
943 15. Kirkpatrick CL, Martins D, Redder P, Frandi A, Mignolet J, Chapalay JB, et al. Growth
944 control switch by a DNA-damage-inducible toxin–antitoxin system in Caulobacter crescentus.
945 Nature Microbiology. 2016;1:16008.

16. LeRoux M, Culviner PH, Liu YJ, Littlehale ML, Laub MT. Stress Can Induce Transcription of Toxin-Antitoxin Systems without Activating Toxin. Molecular Cell. 2020.
17. Fraikin N, Rousseau CJ, Goeders N, Van Melderen L. Reassessing the Role of the Type II MqsRA Toxin-Antitoxin System in Stress Response and Biofilm Formation: mqsA Is Transcriptionally Uncoupled from mqsR. mBio. 2019;10(6):e02678-19.
18. Hallez R, Geeraerts D, Sterckx Y, Mine N, Loris R, Van Melderen L. New toxins homologous to ParE belonging to three-component toxin–antitoxin systems in Escherichia coli O157:H7. Molecular Microbiology. 2010;76(3):719-32.
19. da Rocha RP, Paquola AC, Marques Mdo V, Menck CF, Galhardo RS. Characterization of the SOS regulon of Caulobacter crescentus. J Bacteriol. 2008;190(4):1209-18.
20. Vallet S-U, Hansen LH, Bistrup FC, Laursen SA, Chapalay JB, Chambon M, et al. Loss of Bacterial Cell Pole Stabilization in Caulobacter crescentus Sensitizes to Outer Membrane Stress and Peptidoglycan-Directed Antibiotics. mBio. 2020;11(3):e00538-20.
21. Mets T, Kurata T, Ernits K, Johansson MJO, Craig SZ, Evora GM, et al. Mechanism of phage sensing and restriction by toxin-antitoxin-chaperone systems. Cell host & microbe. 2024;32(7):1059-73.e8.
22. Bordes P, Cirinesi A-M, Ummels R, Sala A, Sakr S, Bitter W, Genevaux P. SecB-like chaperone controls a toxin–antitoxin stress-responsive system in *Mycobacterium tuberculosis*. Proceedings of the National Academy of Sciences. 2011;108(20):8438-43.
23. Nikolskaya AN, Galperin MY. A novel type of conserved DNA-binding domain in the transcriptional regulators of the AlgR/AgrA/LytR family. Nucleic Acids Res. 2002;30(11):2453-9.
24. de la Hoz AB, Ayora S, Sitkiewicz I, Fernández S, Pankiewicz R, Alonso JC, Ceglowski P. Plasmid copy-number control and better-than-random segregation genes of pSM19035 share a common regulator. Proceedings of the National Academy of Sciences. 2000;97(2):728-33.
25. Zhou B, Schrader JM, Kalogeraki VS, Abeliuk E, Dinh CB, Pham JQ, et al. The global regulatory architecture of transcription during the Caulobacter cell cycle. PLoS Genet. 2015;11(1):e1004831.
26. Saha CK, Sanches Pires R, Brolin H, Delannoy M, Atkinson GC. FlaGs and webFlaGs: discovering novel biology through the analysis of gene neighbourhood conservation. Bioinformatics. 2021;37(9):1312-4.
27. Ely B. Evolutionary history of Caulobacter toxin–antitoxin systems. Current Microbiology. 2021;78(8):2899-904.
28. Leplae R, Geeraerts D, Hallez R, Guglielmini J, Drèze P, Van Melderen L. Diversity of bacterial type II toxin–antitoxin systems: a comprehensive search and functional analysis of novel families. Nucleic Acids Research. 2011;39(13):5513-25.
29. Modell JW, Hopkins AC, Laub MT. A DNA damage checkpoint in Caulobacter crescentus inhibits cell division through a direct interaction with FtsW. Genes Dev. 2011;25(12):1328-43.
30. Hocking J, Priyadarshini R, Takacs CN, Costa T, Dye NA, Shapiro L, et al. Osmolality-dependent relocation of penicillin-binding protein PBP2 to the division site in Caulobacter crescentus. J Bacteriol. 2012;194(12):3116-27.
31. Jensen RB, Shapiro L. The Caulobacter crescentus smc gene is required for cell cycle progression and chromosome segregation. Proceedings of the National Academy of Sciences. 1999;96(19):10661-6.
32. Heinrich K, Sobetzko P, Jonas K. A Kinase-Phosphatase Switch Transduces Environmental Information into a Bacterial Cell Cycle Circuit. PLOS Genetics. 2016;12(12):e1006522.
33. Gray WT, Govers SK, Xiang Y, Parry BR, Campos M, Kim S, Jacobs-Wagner C. Nucleoid Size Scaling and Intracellular Organization of Translation across Bacteria. Cell. 2019;177(6):1632-48.e20.

34. Arias-Cartin R, Dobihal GS, Campos M, Surovtsev IV, Parry B, Jacobs-Wagner C. Replication fork passage drives asymmetric dynamics of a critical nucleoid‐associated protein in Caulobacter. The EMBO Journal. 2017;36(3):301-18-18.
35. Ward D, Newton A. Requirement of topoisomerase IV parC and parE genes for cell cycle progression and developmental regulation in Caulobacter crescentus. Molecular Microbiology. 1997;26(5):897-910.
36. Calkins AL, Demey LM, Karslake JD, Donarski ED, Biteen JS, DiRita VJ. Independent Promoter Recognition by TcpP Precedes Cooperative Promoter Activation by TcpP and ToxR. mBio. 2021;12(5):e0221321.
37. Gebhard S, Gaballa A, Helmann JD, Cook GM. Direct stimulus perception and transcription activation by a membrane-bound DNA binding protein. Molecular Microbiology. 2009;73(3):482-91.
38. Merritt J, Zheng L, Shi W, Qi F. Genetic characterization of the hdrRM operon: a novel high-cell-density-responsive regulator in Streptococcus mutans. Microbiology (Reading). 2007;153(Pt 8):2765-73.
39. Xie Z, Okinaga T, Niu G, Qi F, Merritt J. Identification of a novel bacteriocin regulatory system in Streptococcus mutans. Molecular Microbiology. 2010;78(6):1431-47.
40. Zou Z, Qin H, Brenner AE, Raghavan R, Millar JA, Gu Q, et al. LytTR Regulatory Systems: A potential new class of prokaryotic sensory system. PLoS Genet. 2018;14(10):e1007709.
41. Xie Z, Zou Z, Raz A, Qin H, Fischetti V, Zhang S, et al. Regulatory control of the Streptococcus mutans HdrRM LytTR Regulatory System functions via a membrane sequestration mechanism. Mol Microbiol. 2020;114(4):681-93.
42. Demey LM, Gumerov VM, Xing J, Zhulin IB, DiRita VJ. Transmembrane Transcription Regulators Are Widespread in Bacteria and Archaea. Microbiology Spectrum. 2023;11(3):e00266-23.
43. Thanbichler M, Iniesta AA, Shapiro L. A comprehensive set of plasmids for vanillate- and xylose-inducible gene expression in Caulobacter crescentus. Nucleic Acids Res. 2007;35(20):e137.
44. Ardissone S, Fumeaux C, Bergé M, Beaussart A, Théraulaz L, Radhakrishnan SK, et al. Cell cycle constraints on capsulation and bacteriophage susceptibility. eLife. 2014;3:e03587.
45. Viollier PH, Thanbichler M, McGrath PT, West L, Meewan M, McAdams HH, Shapiro L. Rapid and sequential movement of individual chromosomal loci to specific subcellular locations during bacterial DNA replication. Proc Natl Acad Sci U S A. 2004;101(25):9257-62.
46. Simon R, Priefer U, Pühler A. A broad host range mobilization system for *in vivo* genetic engineering: transposon mutagenesis in Gram negative bacteria. Bio/Technology. 1983;1:784-91.
47. Ely B. Genetics of Caulobacter crescentus. Methods Enzymol. 1991;204:372-84.
48. Fumeaux C, Radhakrishnan SK, Ardissone S, Theraulaz L, Frandi A, Martins D, et al. Cell cycle transition from S-phase to G1 in Caulobacter is mediated by ancestral virulence regulators. Nature communications. 2014;5:4081.
49. Cserzo M, Wallin E, Simon I, von Heijne G, Elofsson A. Prediction of transmembrane alpha-helices in prokaryotic membrane proteins: the dense alignment surface method. Protein Eng. 1997;10(6):673-6.
50. Senior AW, Evans R, Jumper J, Kirkpatrick J, Sifre L, Green T, et al. Improved protein structure prediction using potentials from deep learning. Nature. 2020;577(7792):706-10.
51. Katoh K, Misawa K, Kuma Ki, Miyata T. MAFFT: a novel method for rapid multiple sequence alignment based on fast Fourier transform. Nucleic Acids Research. 2002;30(14):3059-66.
52. Tamura K, Stecher G, Kumar S. MEGA11: Molecular Evolutionary Genetics Analysis Version 11. Molecular Biology and Evolution. 2021;38(7):3022-7.

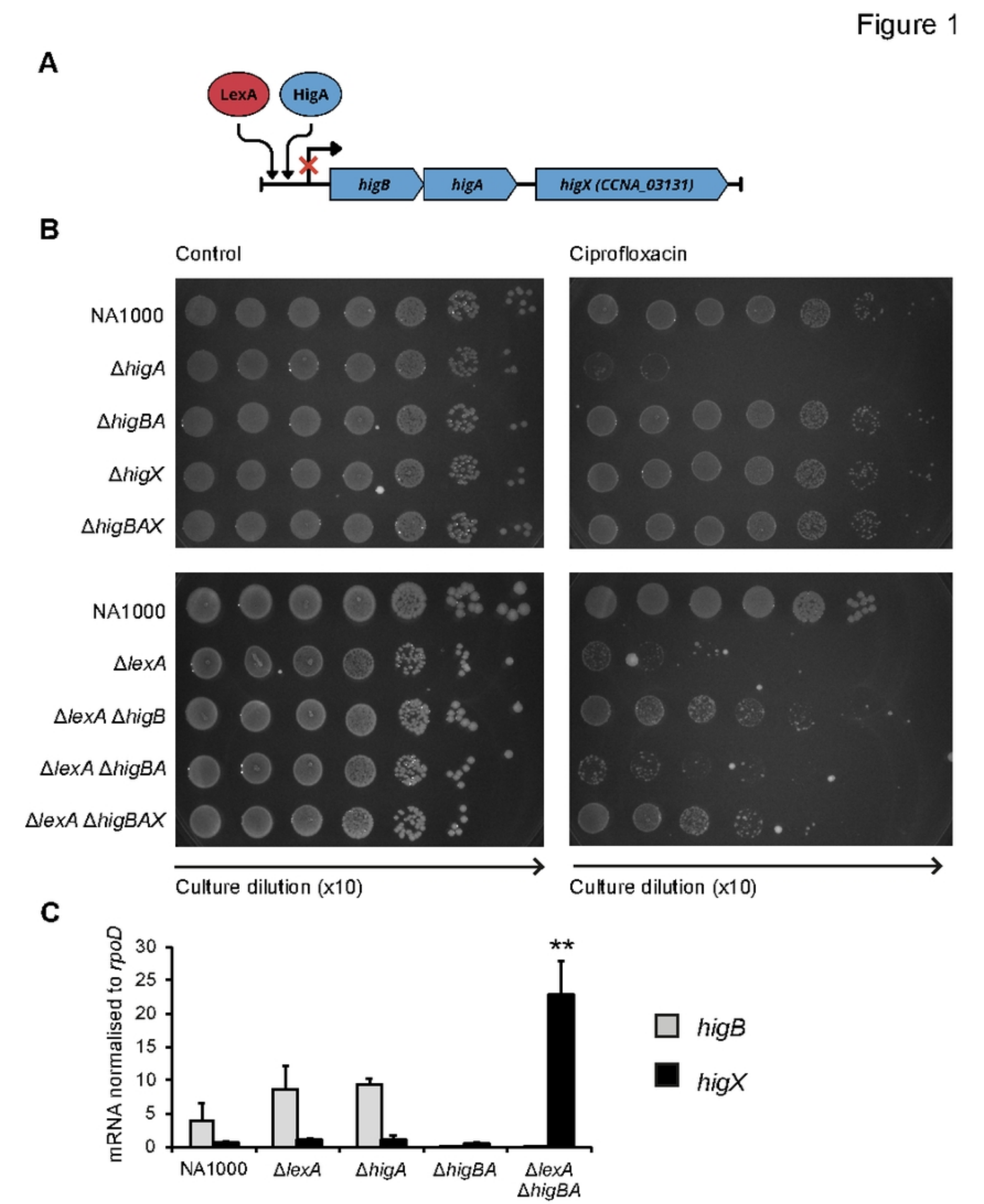
A
LexA
HigA
higB
higA
higX (CCNA_03131)
B
Control
Ciprofloxacin
NA1000
ΔhigA
ΔhigBA
ΔhigX
ΔhigBAX
NA1000
ΔlexA
ΔlexA ΔhigB
ΔlexA ΔhigBA
ΔlexA ΔhigBAX
Culture dilution (x10)
Culture dilution (x10)
C
mRNA normalised to rpoD
30
25
20
15
10
5
0
**
NA1000
ΔlexA
ΔhigA
ΔhigBA
ΔlexA ΔhigBA
higB
higX

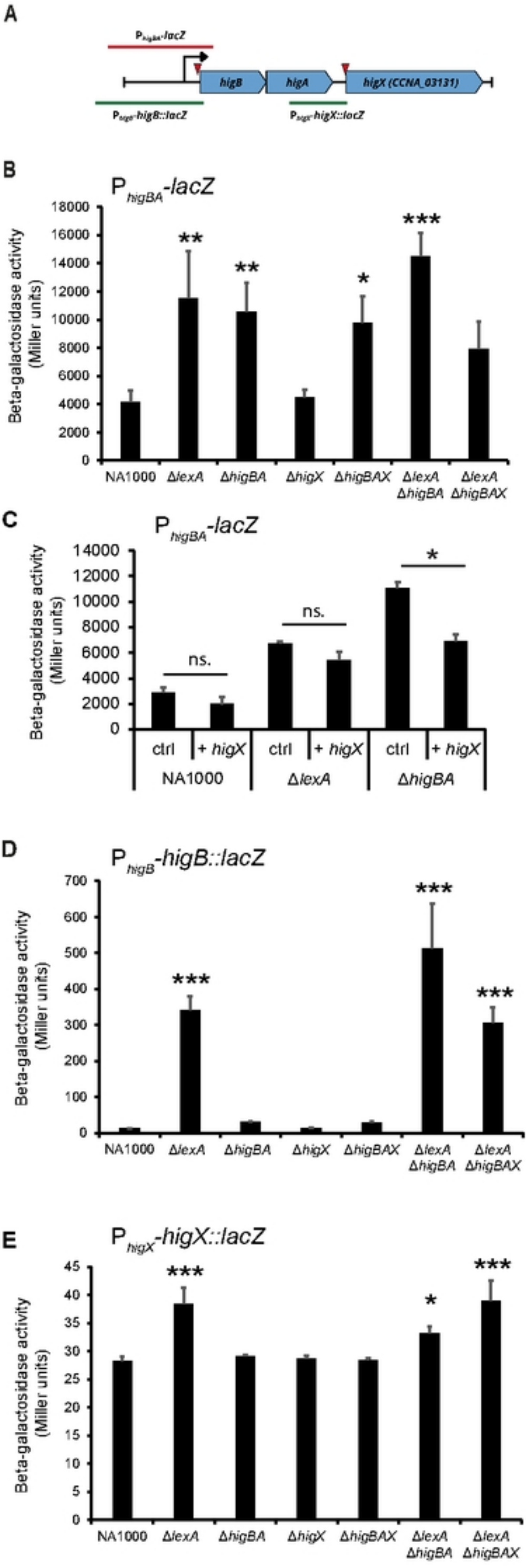
A
P higBA-lacZ
higB
higA
higX (CCNA_03131)
P higB-higB::lacZ
P higX-higX::lacZ
B
P higBA-lacZ
Beta-galactosidase activity (Miller units)
18000
16000
14000
12000
10000
8000
6000
4000
2000
0
**
**
*
***
NA1000
ΔlexA
ΔhigBA
ΔhigX
ΔhigBAX
ΔlexA ΔhigBA
ΔlexA ΔhigBAX
C
P higBA-lacZ
Beta-galactosidase activity (Miller units)
14000
12000
10000
8000
6000
4000
2000
0
ns.
ns.
*
ctrl
+ higX
ctrl
+ higX
ctrl
+ higX
NA1000
ΔlexA
ΔhigBA
D
P higB-higB::lacZ
Beta-galactosidase activity (Miller units)
700
600
500
400
300
200
100
0
***
***
***
NA1000
ΔlexA
ΔhigBA
ΔhigX
ΔhigBAX
ΔlexA ΔhigBA
ΔlexA ΔhigBAX
E
P higX-higX::lacZ
Beta-galactosidase activity (Miller units)
45
40
35
30
25
20
15
10
5
0
***
*
***
NA1000
ΔlexA
ΔhigBA
ΔhigX
ΔhigBAX
ΔlexA ΔhigBA
ΔlexA ΔhigBAX

Figure 2

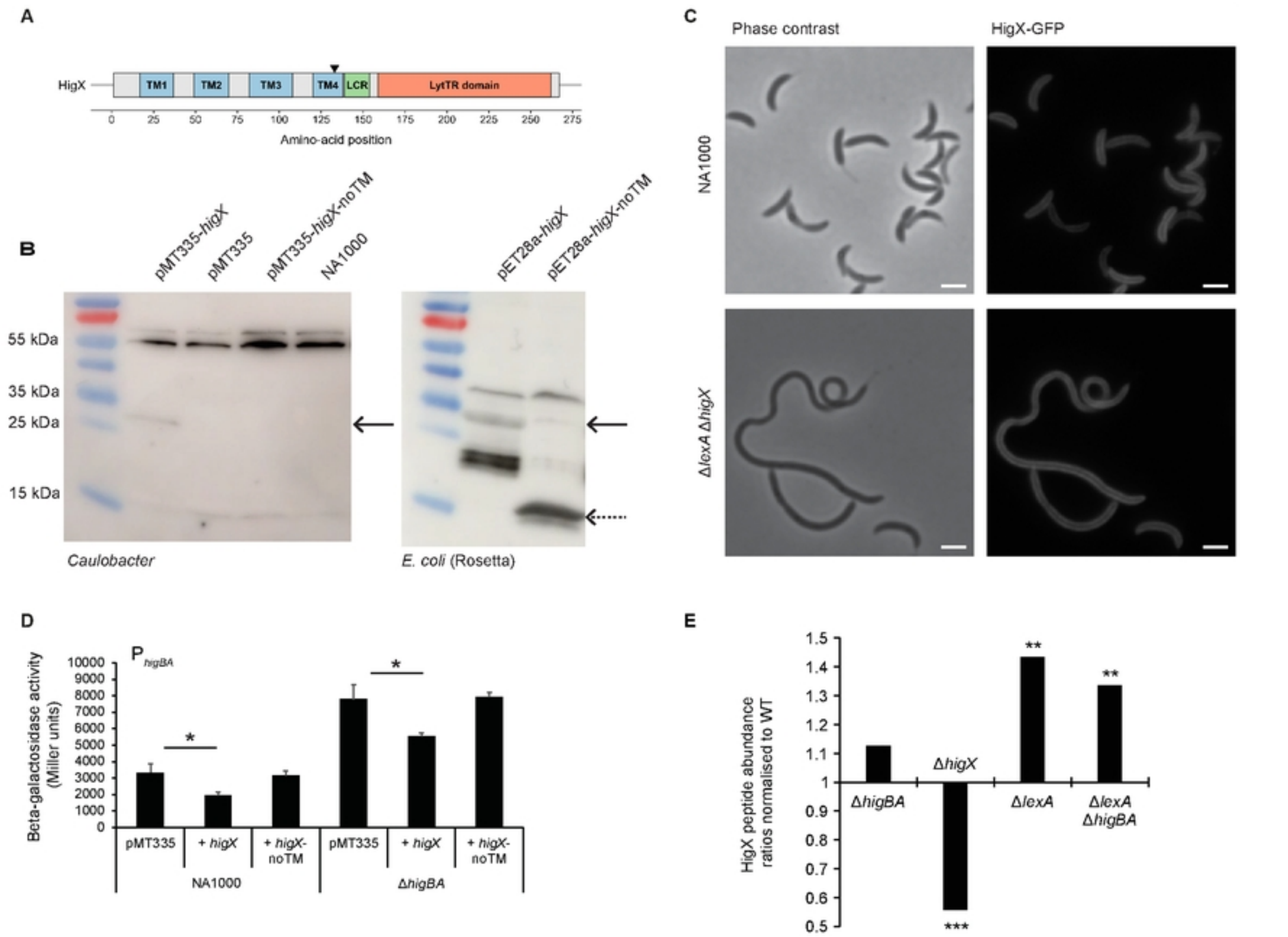
A
HigX
TM1
TM2
TM3
TM4
LCR
LytTR domain
0 25 50 75 100 125 150 175 200 225 250 275
Amino-acid position
B
pMT335-higX
pMT335
pMT335-higX-noTM
NA1000
pET28a-higX
pET28a-higX-noTM
55 kDa
35 kDa
25 kDa
15 kDa
Caulobacter
E. coli (Rosetta)
C
Phase contrast
HigX-GFP
NA1000
ΔlexA ΔhigX
D
P higBA
Beta-galactosidase activity (Miller units)
10000 9000 8000 7000 6000 5000 4000 3000 2000 1000 0
*
*
pMT335
+ higX
+ higX-noTM
pMT335
+ higX
+ higX-noTM
NA1000
ΔhigBA
E
HigX peptide abundance ratios normalised to WT
1.5 1.4 1.3 1.2 1.1 1 0.9 0.8 0.7 0.6 0.5
ΔhigBA
ΔhigX
ΔlexA
ΔlexA ΔhigBA
**
**
***

Figure 3

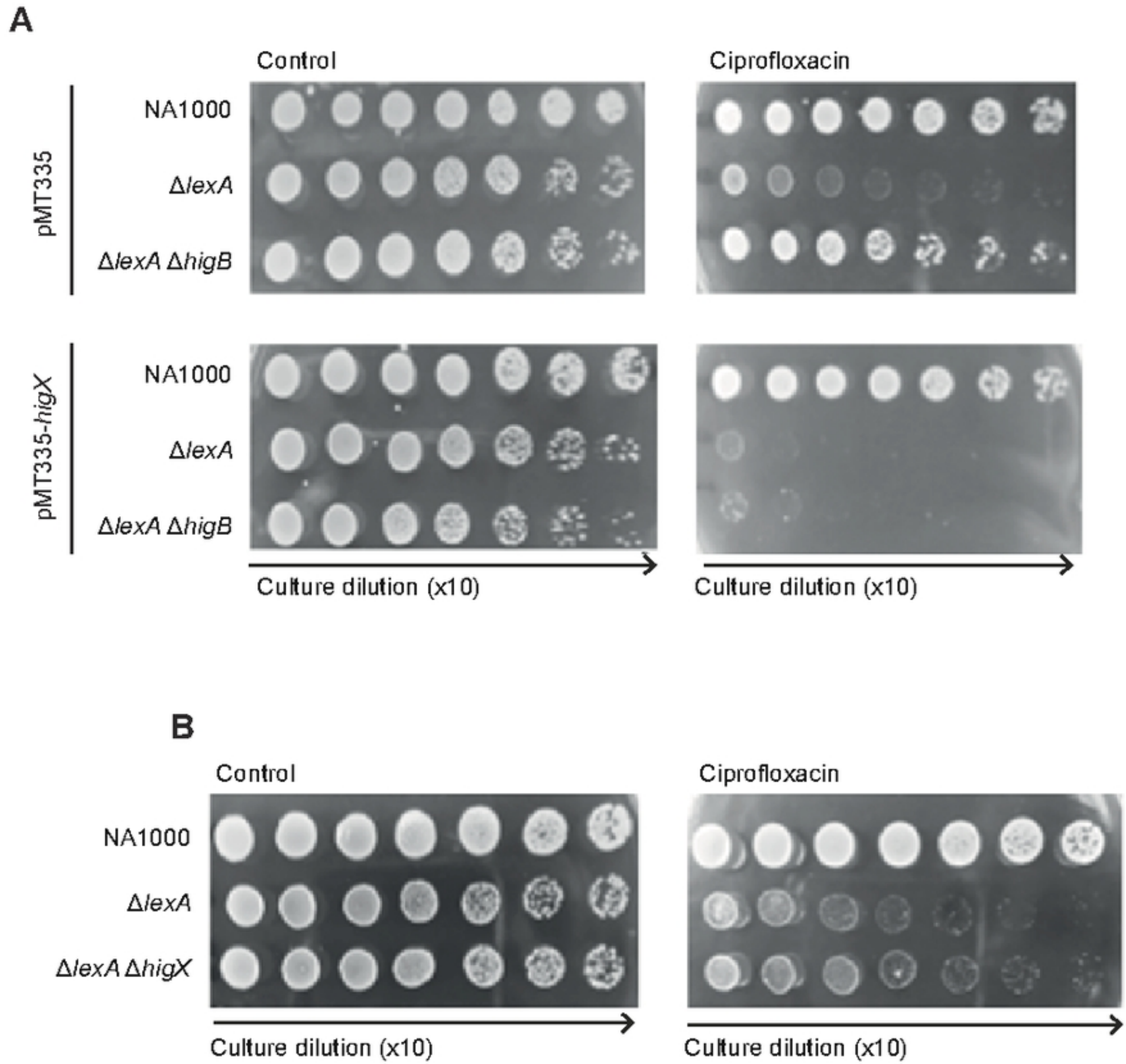
A
Control
Ciprofloxacin
pMT335
NA1000
ΔlexA
ΔlexA ΔhigB
pMT335-higX
NA1000
ΔlexA
ΔlexA ΔhigB
Culture dilution (x10)
Culture dilution (x10)
B
Control
Ciprofloxacin
NA1000
ΔlexA
ΔlexA ΔhigX
Culture dilution (x10)
Culture dilution (x10)

Figure 4

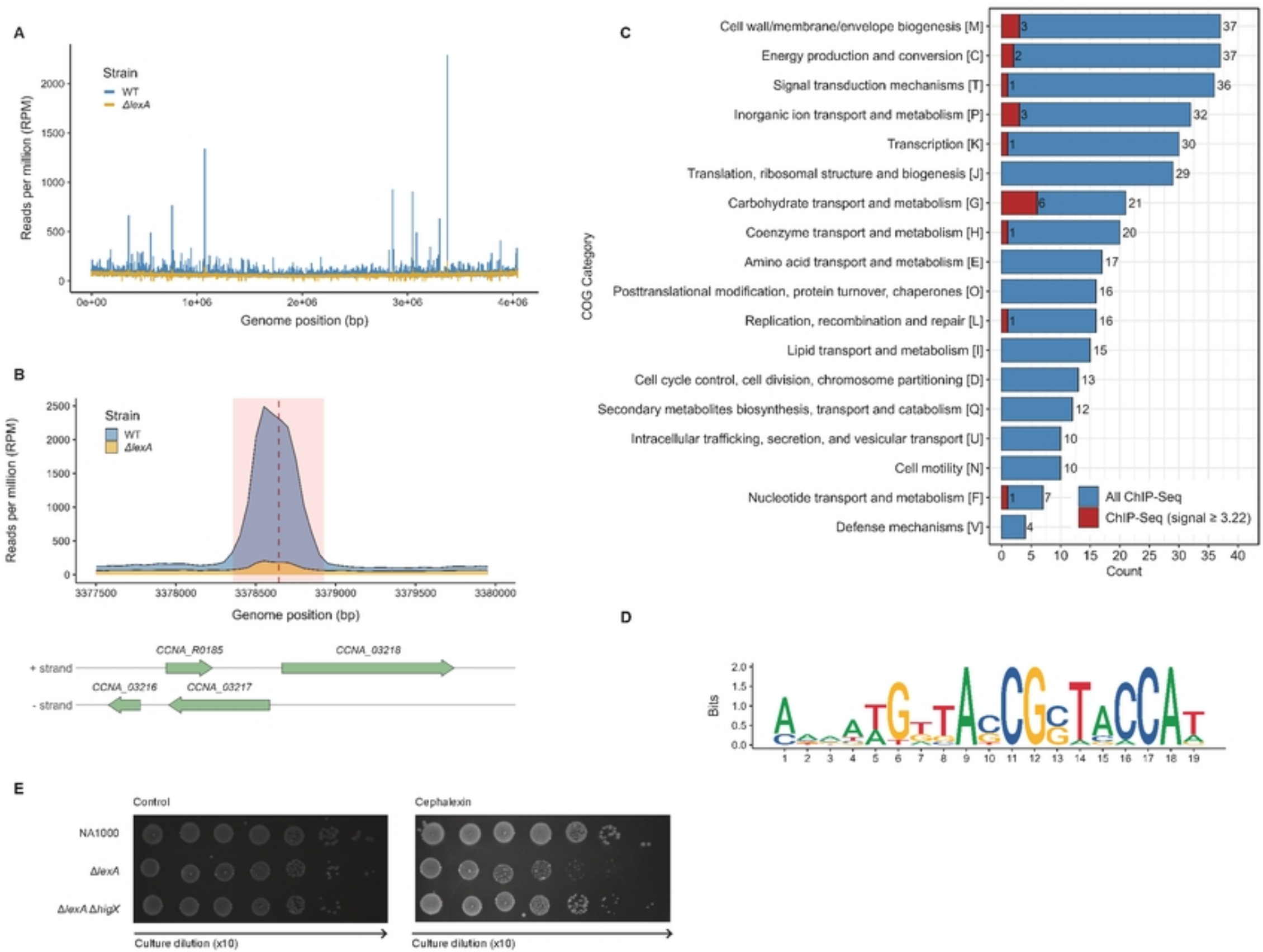
A
Strain
WT
ΔlexA
Reads per million (RPM)
Genome position (bp)
B
Strain
WT
ΔlexA
Reads per million (RPM)
Genome position (bp)
CCNA_R0185
CCNA_03218
+ strand
CCNA_03216
CCNA_03217
- strand
C
Cell wall/membrane/envelope biogenesis [M]
Energy production and conversion [C]
Signal transduction mechanisms [T]
Inorganic ion transport and metabolism [P]
Transcription [K]
Translation, ribosomal structure and biogenesis [J]
Carbohydrate transport and metabolism [G]
Coenzyme transport and metabolism [H]
Amino acid transport and metabolism [E]
Posttranslational modification, protein turnover, chaperones [O]
Replication, recombination and repair [L]
Lipid transport and metabolism [I]
Cell cycle control, cell division, chromosome partitioning [D]
Secondary metabolites biosynthesis, transport and catabolism [Q]
Intracellular trafficking, secretion, and vesicular transport [U]
Cell motility [N]
Nucleotide transport and metabolism [F]
Defense mechanisms [V]
COG Category
Count
All ChIP-Seq
ChIP-Seq (signal ≥ 3.22)
D
Bits
E
Control
Cephalexin
NA1000
ΔlexA
ΔlexA ΔhigX
Culture dilution (x10)
Culture dilution (x10)

Figure 5

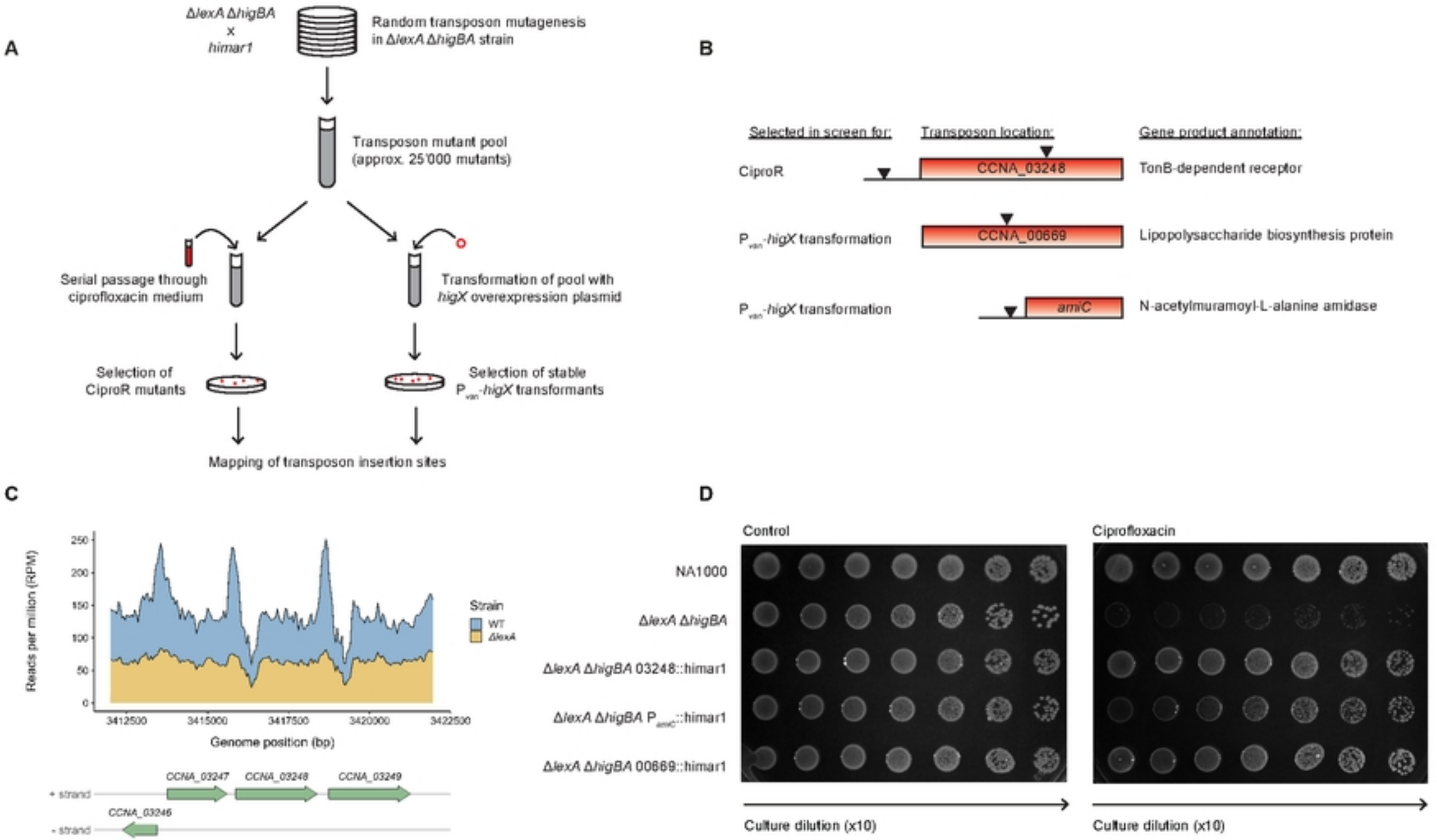
A
ΔlexA ΔhigBA
x
himar1
Random transposon mutagenesis
in ΔlexA ΔhigBA strain
Transposon mutant pool
(approx. 25'000 mutants)
Serial passage through
ciprofloxacin medium
Transformation of pool with
higX overexpression plasmid
Selection of
CiproR mutants
Selection of stable
Pvan-higX transformants
Mapping of transposon insertion sites
B
Selected in screen for:
Transposon location:
Gene product annotation:
CiproR
CCNA_03248
TonB-dependent receptor
Pvan-higX transformation
CCNA_00669
Lipopolysaccharide biosynthesis protein
Pvan-higX transformation
amiC
N-acetylmuramoyl-L-alanine amidase
C
Reads per million (RPM)
Strain
WT
ΔlexA
Genome position (bp)
CCNA_03247
CCNA_03248
CCNA_03249
CCNA_03246
+ strand
- strand
D
Control
Ciprofloxacin
NA1000
ΔlexA ΔhigBA
ΔlexA ΔhigBA 03248::himar1
ΔlexA ΔhigBA Pamic::himar1
ΔlexA ΔhigBA 00669::himar1
Culture dilution (x10)
Culture dilution (x10)

Figure 6

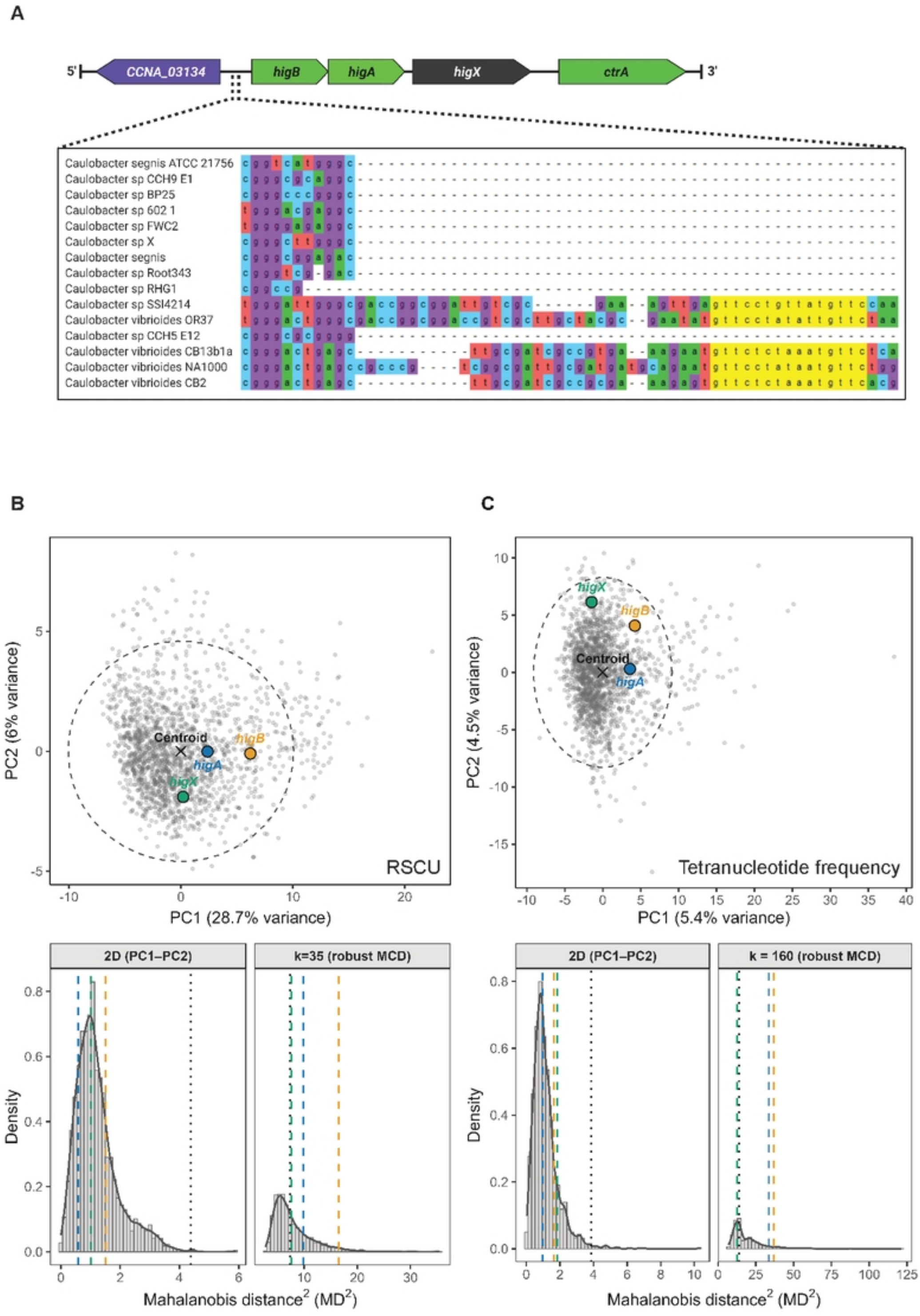
A
5'
CCNA_03134
higB
higA
higX
ctrA
3'
Caulobacter segnis ATCC 21756
Caulobacter sp CCH9 E1
Caulobacter sp BP25
Caulobacter sp 602 1
Caulobacter sp FWC2
Caulobacter sp X
Caulobacter segnis
Caulobacter sp Root343
Caulobacter sp RHG1
Caulobacter sp SSI4214
Caulobacter vibrioides OR37
Caulobacter sp CCH5 E12
Caulobacter vibrioides CB13b1a
Caulobacter vibrioides NA1000
Caulobacter vibrioides CB2
B
PC2 (6% variance)
PC1 (28.7% variance)
Centroid
higB
higA
higX
RSCU
C
PC2 (4.5% variance)
PC1 (5.4% variance)
Centroid
higX
higB
higA
Tetranucleotide frequency
2D (PC1–PC2)
k=35 (robust MCD)
2D (PC1–PC2)
k = 160 (robust MCD)
Density
Mahalanobis distance² (MD²)

Figure 7

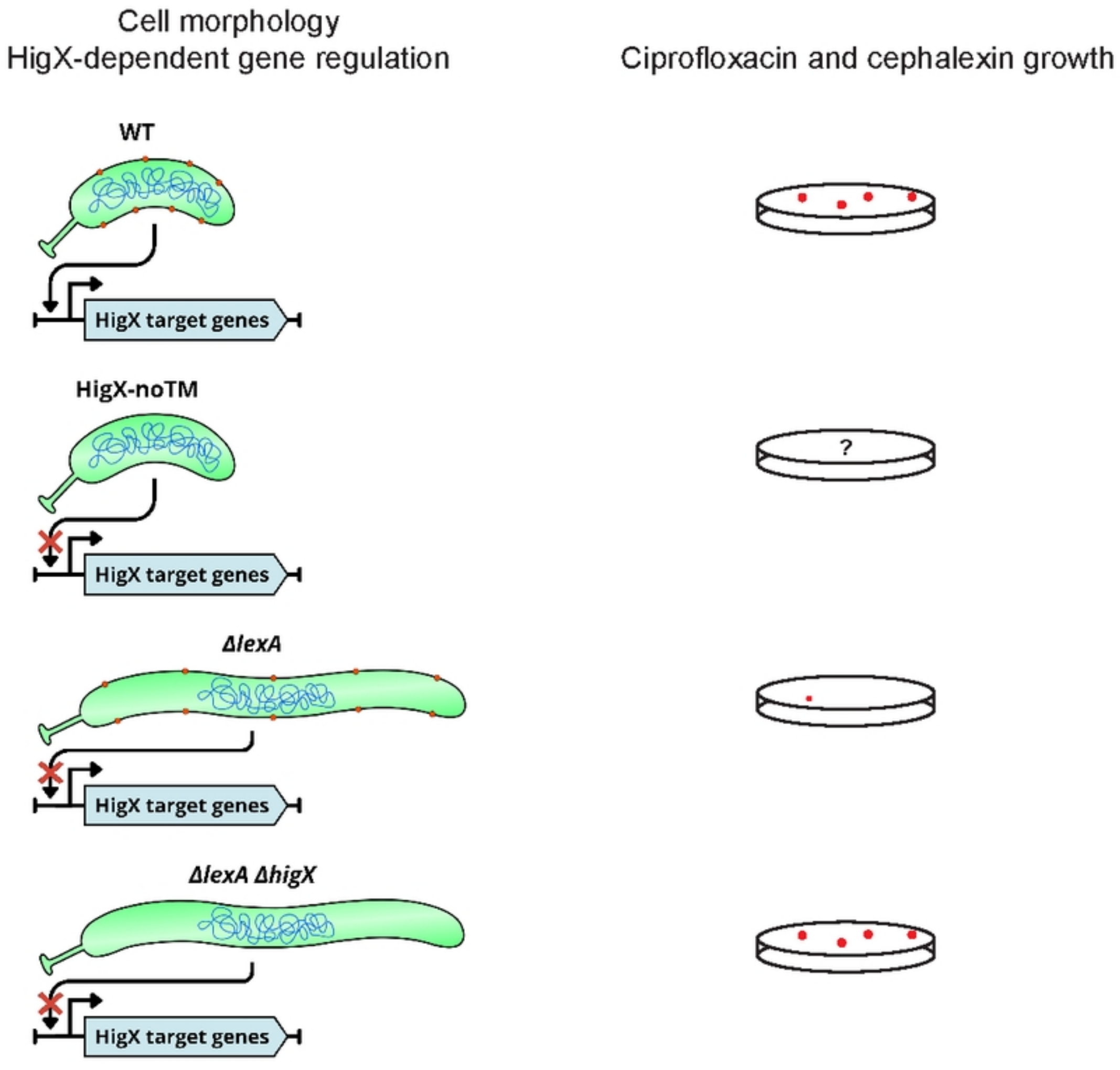
Cell morphology
HigX-dependent gene regulation
Ciprofloxacin and cephalexin growth
WT
HigX target genes
HigX-noTM
?
HigX target genes
ΔlexA
HigX target genes
ΔlexA ΔhigX
HigX target genes

Figure 8